Supporting Information for

# Surface Immobilized Copper(I)diimine Photosensitizers as Molecular Probes for Elucidating the Effects of Confinement at Interfaces for Solar Energy Conversion

*Michael S. Eberhart,[a] Brian T. Phelan,[a] Jens Niklas,[a] Emily A. Sprague-Klein,[a] David M. Kaphan, [a] David J. Gosztola,[b] Lin X. Chen,[a,c] David M. Tiede,[a] Oleg G. Poluektov,[a] and Karen L. Mulfort[a]**

[a]Division of Chemical Sciences and Engineering, Argonne National Laboratory, 9700 South Cass Avenue, Lemont, IL 60439; [b]Center for Nanoscale Materials, Argonne National Laboratory, Lemont, IL 60439; [c]Department of Chemistry, Northwestern University, 2145 Sheridan Rd, Evanston, IL 60208

*To whom correspondence should be addressed. E-mail: mulfort@anl.gov

**Contents**

**Experimental methods.**

*General methods.* $^1$H NMR was performed on a Bruker DMX 500 and referenced to TMS, TSP*, or the residual solvent peak. ESI-MS was collected on a ThermoFisher LCQ Fleet, from dilute methanol solutions in positive ionization mode. High-resolution mass spectrometry was performed at the University of Illinois School of Chemical Sciences Mass Spectrometry Laboratory. UV-vis absorption measurements were performed on a Beckman Coulter DU800 spectrophotometer. AAO wafers were purchased in 40, 20, and 10 nm pore sizes from InRedox (Longmont, CO) and used as received.

*Diffuse Reflectance.* The UV-Vis spectra were obtained on a Shimadzu UV-3600 Plus spectrometer equipped with a PMT (photomultiplier tube) detector. The samples were diluted with polytetrafluoroethylene (PTFE) at a dilution factor of ~10 to 1. The reflectance from the sample was measured from 200 to 800 nm at a medium scan speed with a sampling interval of 1 nm and a slit width of 3 nm. A background spectrum was obtained with a PTFE blank and was subtracted from the sample spectra.

*EPR*. AAO wafers with oxidized immobilized **3** were broken into small pieces and then loaded into quartz EPR tubes, sealed under $N_2$ atmosphere, and cooled in liquid nitrogen. Continuous wave (CW) X-band (9.5 GHz) EPR experiments were carried out with a Bruker ELEXSYS II E500 EPR spectrometer (Bruker Biospin, Rheinstetten, Germany), equipped with a $TE_{102}$ rectangular EPR resonator (Bruker ER 4102ST). A Helium gas-flow cryostat (ICE Oxford, UK) and an ITC (Oxford Instruments, UK) were used for cryogenic temperatures. Data processing was done using Xepr (Bruker BioSpin, Rheinstetten) and Matlab R2018b (The MathWorks, Inc., Natick) environment.

*Electrochemistry*. Cyclic voltammetry was conducted using a standard three-electrode cell on a BioAnalytical Systems (BAS) 100B potentiostat. For the solution phase analysis of 1, a 1.5 mm diameter gold working electrode, a platinum wire counter electrode, and a pseudo Ag/AgCl reference electrode (1.5 mm diameter Ag wire coated with AgCl) were used. Solutions were prepared using anhydrous acetonitrile, purged with $N_2$ prior to measurement, and subsequently maintained under a blanket of $N_2$. Tetrabutylammonium hexafluorophosphate (0.1 M) was used as the supporting electrolyte. Ferrocene (purified by sublimation) was added after the measurement as an internal standard and redox potentials were referenced to the ferrocene/ferrocenium couple (0.40 V vs. SCE (acetonitrile)[1]). For the electrochemical analysis of **1**, **2**, and **3**, the complexes were immobilized on high surface area *nano*ITO working electrodes (described below) immersed in anhydrous acetonitrile containing 0.1 M $nBu_4NPF_6$. A platinum wire was used for the counter electrode and an $Ag/Ag^+$ reference electrode consisting of a silver wire in 10 mM $AgNO_3$ and 0.1 M $nBu_4NPF_6$ in acetonitrile which was separated from the rest of the electrochemical cell by a Vycor frit. At the end of the experiment, sublimation purified ferrocene was added to the experiment solution and its cyclic voltammogram recorded using a 1.5 mm diameter platinum working electrode to verify the potential of the reference electrode. Potentials are reported vs the ferrocene/ferrocenium couple.

*Transient absorption spectroscopy.* Femtosecond transient absorption (fsTA) spectroscopy experiments for **3** on AAO and $TiO_2$ were performed using a 1 kHz Ti:sapphire regeneratively-amplified laser system (Spectra-Physics MaiTai oscillator / Spitfire Pro XP amplifier) which has been described previously.[2, 3] Briefly, 0.6 mJ of the amplified laser pulses (830 nm, 100 fs, 2.8 mJ) were directed towards a 10% reflective beamsplitter. The transmitted fundamental was reduced to a beam diameter of ~2 mm before driving second harmonic generation (SHG) in a 2 mm thick Type I lithium triborate crystal ($\theta = 90°$, $\phi = 28°$) and was then used to pump a laboratory-constructed optical parametric amplifier (OPA) tuned so the signal output was 500 nm.[2] The 60 μJ of fundamental reflected by the beamsplitter prior to SHG was further split, with ~10 μJ directed

towards generating a white light continuum to seed the OPA.[2] The remaining ~50 μJ of fundamental and the signal from the OPA were both directed towards the TA spectrometer (Helios, Ultrafast Systems). The fundamental was directed along an optical delay stage with ~4 μJ focused into a 3 mm thick sapphire window to generate a white light continuum probe ranging from 450-800 nm. The 500 nm pump was directed through a thin-film polarizer, set to magic angle with respect to the probe, and a mechanical chopper, operating at 500 Hz to block every other pulse, and was attenuated to 0.4-0.8 μJ/pulse at the sample. The pump and probe pulses were focused to about 500 μm and 100 μm, respectively, and overlapped in the sample. The probe pulse was collimated and then focused into a fiber optic cable coupled to a CCD detector. The difference spectra were calculated using the Helios software (Ultrafast Systems) via Equation S1

$$S(\lambda, \Delta t) = \langle -\log(I^*/I_o) \rangle \quad \text{(S1)}$$

where $S(\lambda, \Delta t)$ is the difference signal, $I^*$ is the intensity of a single pump-on probe-plus-signal spectrum, and $I_o$ is the intensity of a single pump-off probe spectrum.

Nanosecond transient absorption (nsTA) spectroscopy experiments, also described previously,[3, 4] were performed using a 1 kHz Nd:YAG diode-pumped mode-locked laser (Ekspla PL2210) paired with a 1 kHz supercontinuum laser (Leukos STM-1-UV). An internal pulse picker reduced the Nd:YAG pulse train to 500 Hz and the fundamental was frequency-tripled internally, yielding a 1 kHz train of 355 nm (25 ps, 0.3 mJ) pulses. The third harmonic output pumped an optical parametric generator (Ekspla PG403) tuned so the signal was 500 nm (25 ps, 25 μJ pulses). The supercontinuum laser was synchronized to a 1 kHz trigger from the Nd:YAG laser and output a 1 kHz train of unpolarized broadband laser pulses (350 to 2400 nm, ~600 ps, 15 μJ). The supercontinuum probe pulses were directed through a 950 nm short-pass filter to eliminate the residual 1064 nm fundamental from the supercontinuum laser. The 500 nm pump pulses were attenuated to 0.2-0.3 μJ/pulse and focused to a diameter of ~200 μm and spatially overlapped at the sample with the probe pulses, which were focused to a diameter of ~100 μm. The probe pulses were collimated and focused into an SP-2150i Acton Series spectrograph (Princeton Instruments) with a slit width of 230 μm and a 150 g/mm grating blazed at 800 nm with the spectral window centered at 600 nm. The dispersed light was imaged using a Spyder3 SG-14 (Teledyne DALSA) CCD camera. A laboratory-written application (LabVIEW 2014, National Instruments) provided the time delays to the supercontinuum laser via DG535 delay generators (Stanford Research Systems) that were externally triggered by the master clock and through a series of TTL electronic timing schemes delayed the probe pulse with respect to the pump. The LabVIEW program also recorded the probe pulse spectra and calculated the difference spectra using Equation S2.

$$S(\lambda, \Delta t) = -\log(\langle I^* \rangle / \langle I_o \rangle) \quad \text{(S2)}$$

Equation S2 differs from Equation S1 in that the pump-on probe-plus-signal spectra and pump-off probe spectra are first averaged before the difference spectra are calculated.

The dye-loaded films were placed in a 2 mm quartz cuvette filled with neat dichloromethane. The cuvettes were rastered in two dimensions during the nsTA measurements and in one dimension during the fsTA measurements, using motorized linear actuators (X-NA08A25, Zaber Technologies Inc.), to limit the effects of heating and photodegradation. No sample degradation was observed during the course of the measurements at the fluences used. The fsTA experiments were collected by averaging 350 difference spectra (0.7 s) at each time delay (401 total time delays ranging from -2 to 3150 ps) during a single scan of the delay stage and 6-7 scans of the delay stage were collected in total. The nsTA experiments were collected by averaging 250 difference spectra (0.5 s) at each time delay (500 total time delays ranging from -10 ns to 10 μs or 1000 total time delays ranging from -10

ns to 950 μs) during a single sweep of the full set of time delays and 7-12 scans of the time delays were collected in total. For both the fsTA and nsTA spectra, the background signal and pump scatter were subtracted from the raw data and the spectra were corrected for group delay dispersion in the probe pulse.

Femtosecond transient absorption data for **1**, **2**, and **3** in solution as well as **1** immobilized on AAO were collected at the Center for Nanoscale Materials at Argonne National Laboratory using an amplified Ti:Sapphire laser system (Spectra Physics, Spitfire Pro) and an automated data acquisition system (Ultrafast Systems, Helios). The amplifier was seeded with the 100 fs output from the oscillator (Spectra Physics, Tsunami) and was operated at 5.0 kHz, giving 0.6 mJ pulses centered at 790 nm. The beam was split 90/10, with the weaker beam being used to generate the white light continuum (440 to 760 nm) probe after traversing a motorized delay stage by being focused into a sapphire plate. The continuum probe was focused to a spot size of 200 μm at the sample and subsequently focused into a fiber optic coupled to a multichannel spectrometer and CMOS sensor. The other 790 nm beam was used to pump an optical parametric amplifier (OPA, Light Conversion, TOPAS). The OPA was tuned to 1680 nm and its output was quadrupled, giving 420 nm pump beam. This beam was passed through a depolarizer, synchronously chopped at 2500 Hz, focused at the sample position to a spot size of 400 μm, and attenuated to a pulse energy of 0.2-.3 μJ. Transient absorption spectra were collected using the Helios control software. The data were corrected for temporal chirp in the probe beam. All experiments were performed at room temperature in 1 or 2 mm quartz cuvettes that had been bubbled with nitrogen. The samples were 1D rastered to limit sample degradation.

**Synthesis schemes and synthesis details.**

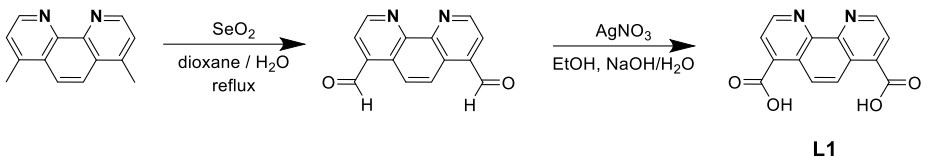


**Scheme S1.** Synthesis of **L1**.

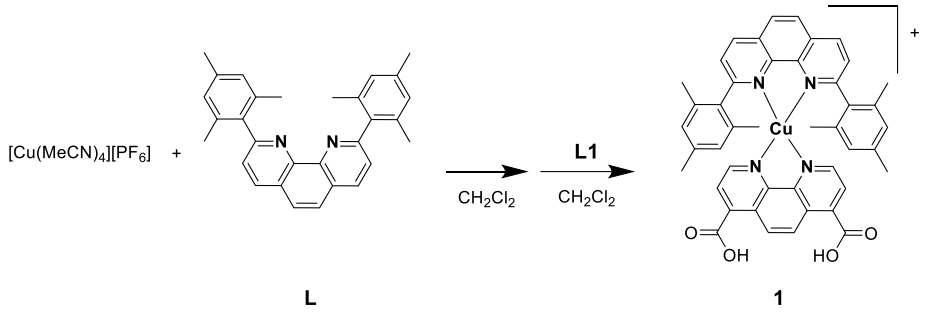


**Scheme S2.** Synthesis of **1**.

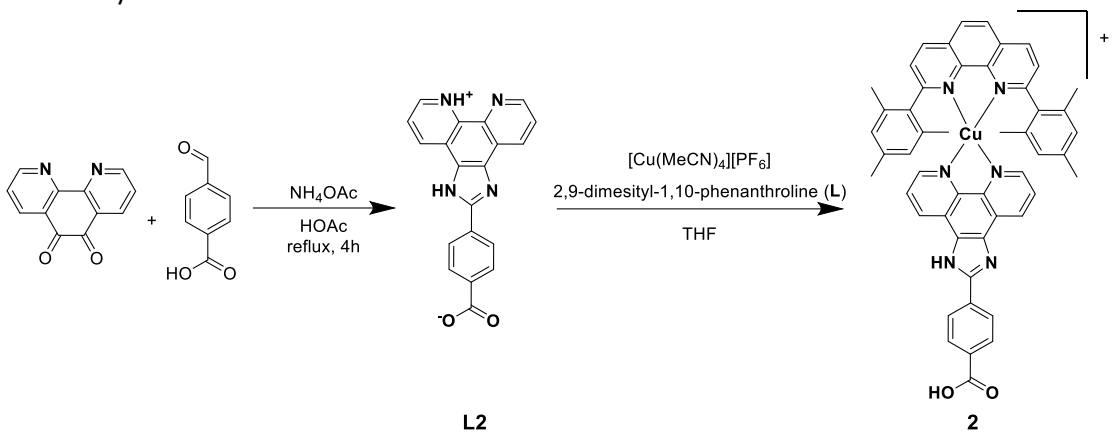


**Scheme S3.** Synthesis of **L2** and **2**.

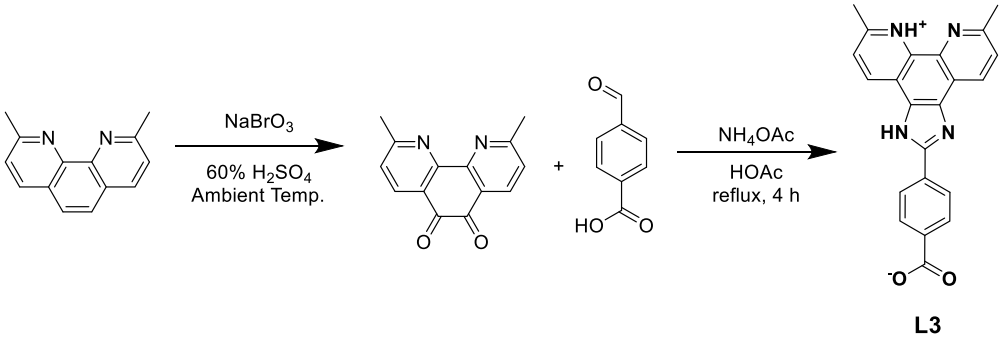


**Scheme S4.** Synthesis of **L3**.

**Synthesis details.**

*General considerations.* All reagents and solvents were purchased from commercial sources and were used as received except those described below.

*Synthesis of 2,9-dimesityl-1,10-phenanthroline* (**L**). The blocking ligand **L** was synthesized as described previously in the literature[5] or by a modified procedure using (dppf)$PdCl_2$ which allows for lower catalyst loading. 2,9-dichlorophenanthroline (3 g, 12 mmol), mesitylboronic acid (4.737 g, 29 mmol), toluene (245 mL), water (105 mL), and sodium carbonate (22.26 g, 210 mmol to give 2 M aqueous concentration) were added to a vessel along with a stir bar and sparged with $N_2$. Dppf(Pd)$Cl_2$ (441 mg, 5 mol%), was then added and the reaction was heated under inert atmosphere to 80 °C for 20 hours. The reaction was allowed to cool, dichloromethane was added and the aqueous layer was extracted twice more with dichloromethane. The combined organic layers were dried with $MgSO_4$ and partially rotovapped to remove the dichloromethane and some of the toluene. The solution was cooled to induce precipitation and the target compound was collected as a white solid with a medium frit, 3.25 g, 7.8 mmol, 65%). $^1$H NMR (500 MHz, $CDCl_3$) δ = 8.28 (d, *J* = 8.2 Hz, 2H), 7.86 (s, 2H), 7.58 (d, *J* = 8.2 Hz, 2H), 6.93 (s, 4H), 2.31 (s, 6 Hz), 1.63 (s, 12H).

*Synthesis of **L1**.* 1,10-phenanthroline-4,7-dicarbaldehyde was synthesized by literature procedure.[6] 4,7-dimethyl-1,10-phenanthroline (1.05 g, 4.8 mmol), selenium dioxide (2.66 g, 24 mmol), 67 mL dioxane, and 2.68 g water (4 wt%) were heated at reflux for 2.5 hours, filtered hot, and allowed to cool. The filtrate was reheated to redissolve the product and allowed to cool to room temperature, yielding tan crystals which were collected on a frit and washed with THF, hexanes, and ether. A small amount of 4-formyl,7-methyl-phenanthroline was observed by NMR and may be overrepresented in the NMR spectrum due to greater solubility, its presence did not complicate synthesis or purification of **L1**. $^1$H NMR (500 MHz, DMSO-$d_6$) δ = 10.70 (s, 2H), 9.47 (d, *J* = 4.3 Hz, 2H), 9.14 (s, 2H), 8.28 (d, *J* = 4.3 Hz, 2H)

1,10-phenanthroline-4,7-dicarboxylic acid (**L1**) was synthesized by a route similar to that described in the literature for related compounds.[7-9] 1,10-phenanthroline-4,7-dicarbaldehyde (130 mg) was suspended in 5 mL absolute ethanol. A solution of silver nitrate (206 mg, 1.21 mmol) in 1 mL water and 4.1 mL 1 M sodium hydroxide were added. The black suspension was stirred for 16 hours, filtered with a fine frit and washed with 1.0 M sodium hydroxide. 2.0 M HCl was used to adjust the pH of the filtrate to 4 resulting in a white precipitate which was collected on a frit (99 mg, 0.38 mmol, 68%). NMR spectra matched those in the literature.[10] $^1$H NMR (500 MHz, $D_2O$/NaOD) δ = 9.06 (d, *J* = 4.6 Hz, 2H), 8.20 (s, 2H), 7.78 (d, *J* = 4.6 Hz, 2H). TSP* was used as an internal standard to reference the spectrum.

*Synthesis of copper(I)(2,9-dimesityl-1,10-phenanthroline)(4,7-dicarboxylic acid-1,10-phenanthroline) hexafluorophosphate* (**1**). Following the "HETPHEN" method for synthesis of heteroleptic copper(I)bis(phen) complexes, tetrakis(acetonitrile)Copper(I) hexafluorophosphate (37 mg) was dissolved in dichloromethane (10 mL) and sparged with nitrogen for 10 minutes. 2,9-dimesitylphenanthroline (42 mg) in 10 mL degassed $CH_2Cl_2$ was added while maintaining a blanket of nitrogen and stirred under nitrogen for five minutes. 1,10-phenanthroline-4,7-dicarboxylic acid (**L1**) (27 mg) was then added and the reaction mixture was stirred at ambient temperature under nitrogen overnight. The red solution was filtered to remove some insoluble material. The dichloromethane was removed by rotary evaporation and the red solid was re-dissolved in a minimal amount of dichloromethane and layered with ether. The product was collected on a frit (43 mg, 5.74 x $10^{-5}$ mol, yield 51%). $^1$H NMR (500 MHz, methanol-$d_4$ with NaOD) δ = 8.82 (d, *J* = 8.2 Hz, 2H), 8.53 (d, *J* = 4.8 Hz, 2H), 8.51 (s, 2H), 8.29 (s, 2H), 7.90 (d, *J* = 8.2 Hz, 2H), 7.79 (d, *J* = 4.85 Hz, 2H), 6.07 (s, 4H), 1.75 (s, 12H), 1.66 (s, 6H). HRMS ESI $C_{44}H_{36}N_4O_4Cu^+$ calcd 747.2033; found 747.2032.

*Synthesis of 4-(1H-imidazo[4,5-f][1,10]phenanthrolin-2-yl)benzoic acid (**L2**)•HOAc*. 1,10-Phenanthroline-5,6-dione (525 mg, 2.5 mmol), ammonium acetate (3.85 g, 50 mmol), terephthalaldehydic acid (525 mg, 3.5 mmol), and acetic acid (10 mL) were added to a vessel equipped with a stir bar and heated to reflux for 4 hours. The reaction mixture was cooled to room temperature and diluted with water. The yellow product was collected on a medium frit and washed with water, ethanol, and dichloromethane. (920 mg, 92%) $^{1}$H NMR (500 MHz, DMSO-$d_6$) δ = 13.98 (s, 1H), 9.08-9.04 (br mult, 2H), 8.98-8.93 (br mult, 2H), 8.42 (d, *J* = 8.3 Hz, 2H), 8.18 (d, *J* = 8.4 Hz, 2H), 7.92-7.82 (mult., 2H), 1.91 (s, 1H). $^{13}$C NMR (125 MHz, DMSO-$d_6$) 172.1, 167.0, 149.4, 148.1, 143.7, 133.7, 131.3, 130.1, 129.8, 126.2, 123.6, 21.1.

*Synthesis of Copper(I)(2,9-dimesityl-1,10-phenanthroline)[4-(1H-imidazo[4,5-f][1,10]phenanthrolin-2-yl)benzoic acid] hexafluorophosphate (**2**).* Tetrakis(acetonitrile)Copper(I) hexafluorophosphate (111 mg) was dissolved in 30 mL THF and sparged with $N_2$. 2,9-dimesityl-1,10-phenanthroline (**L**) (123 mg) was then added, resulting in immediate formation of a yellow solution and stirred for five minutes before addition of one equivalent of **L2** (100 mg). The reaction was stirred for one hour and the THF was removed by rotary evaporation. The red product was dissolved in a minimal amount of dichloromethane, layered with ether, and allowed to stand overnight. We obtained a small quantity of deep red crystals (25 mg) which were used for further studies and were pure by NMR and mass spectrometry. The crystallization conditions promoted ligand dissociation, resulting in decomposition which resulted in a white precipitate consisting of **L2** which was discarded and 2,9-dimesityl-1,10-phenanthroline was observed in the mother liquor by mass spectrometry. The complex appears to be more stable in methanol than dichloromethane. (25 mg, 2.6 x $10^{-5}$ mol, 9%) $^{1}$H NMR (500 MHz, DMSO-$d_6$) δ = 9.02 (d, *J* = 8.1 Hz ,2H), 8.95 (d, *J* = 8.2 Hz, 2H), 8.66-8.59 (br mult., 2H), 8.44 (d, *J* = 7.7 Hz, 2H), 8.40 (s, 2H), 8.22 (d, *J* = 7.7 Hz, 2H), 7.99 (d, *J* = 8.3 Hz, 2H), 8.01-7.86 (br mult., 2H) 6.00-5.95 (br mult., 4H), 1.73-1.66 (apparent d, 12H), 1.39 (s, 6 H). $^{13}$C NMR (125 MHz, methanol-$d_4$) δ = 160.8, 145.2, 142.8, 139.7, 139.2, 138.7, 138.2, 136.3, 135.8, 131.3, 130.0, 128.7, 128.4, 128.3, 20.7, 20.6, 20.4. HRMS ESI $C_{50}H_{40}N_6O_2Cu^+$ calcd 819.2509 found 819.2502.

*2,9-dimethyl-1,10-phenanthroline-5,6-dione* was synthesized by a slightly modified literature procedure.[11] Neocuproine (2.38 g, 10 mmol) was dissolved in 23 mL 60 wt% sulfuric acid. Sodium bromate (1.66 g, 11 mmol) was slowly added while the reaction mixture was stirred. The reaction was stirred overnight at ambient temperature. The reaction mixture was poured into water and neutralized with solid sodium bicarbonate followed by extraction (3x) with dichloromethane. The combined organic layers were dried with magnesium sulfate and the solvent was removed by rotary evaporation yielding a yellow oil that crystallized upon standing. The crystals were washed with ether (1.42g, 60%). $^{1}$H NMR (500 MHz, $CDCl_3$) δ = 8.38 (d, *J* = 8.0 Hz, 2H), 7.42 (d, *J* = 8.0 Hz, 2H), 2.85 (s, 6H).

*Synthesis of 4-(6,9-dimethyl-1H-imidazo[4,5-f][1,10]phenanthrolin-2-yl)benzoic acid (**L3**)•HOAc.* 2,9-dimethyl-1,10-phenanthroline-5,6-dione (477 mg, 2 mmol), ammonium acetate (3.08 g, 40 mmol), terephthalaldehydic acid (360 mg, 2.4 mmol), and 50 mL glacial acetic acid were added to a vessel equipped with a stir bar and heated to reflux for 4 hours. The reaction mixture was cooled to room temperature and diluted with water. The yellow product was collected on a medium frit and washed with water, ethanol, and dichloromethane. (821 mg, 96%) $^{1}$H NMR (500 MHz, methanol-$d_4$ +NaOD) δ = 8.95 (d, J = 8.3 Hz, 2H), 8.34 (d, J = 8.4, 2H), 8.06 (d, J = 8.2, 2H), 7.57 (d, *J* = 8.3 Hz, 2H), 2.85 (s, 6H). $^{13}$C NMR (125 MHz, DMSO-$d_6$) δ = 156.2, 149.0, 143.0, 130.0, 126.0, 123.3, 30.7, 24.9

*Synthesis of Copper(I)(2,9-dimesityl-1,10-phenanthroline) [4-(6,9-dimethyl-1H-imidazo[4,5-f][1,10]phenanthrolin-2-yl)benzoic acid] (**3**)*. Tetrakis(acetonitrile)Copper(I) hexafluorophosphate (111 mg) was dissolved in 30 mL THF and sparged with $N_2$. 2,9-dimesityl-1,10-phenanthroline (**L**)

(123 mg) was then added, resulting in immediate formation of a yellow solution and stirred for five minutes before addition of **L3** (109 mg). The reaction was stirred overnight and the THF removed by rotary evaporation. The red product was dissolved in acetone and precipitated with ether. Dynamic interactions between the 2,9-dimesityl-1,10-phenanthroline ligand and **L3** complicate assignment of the $^{1}$H NMR spectrum. (200 mg, 68%) $^{1}$H NMR (500 MHz, methanol-$d_4$) δ = 9.17 (br s), 8.97-8.80 (mult.), 8.34 (mult.), 8.17 (br s), 8.07 (br s), 7.99-7.89 (mult.), 6.65 (br s), 6.32 (br s), 6.00 (br s), 1.90-1.48 (mult.). $^{13}$C NMR (125 MHz, methanol-$d_4$) δ = 145.3, 145.2, 141.4, 139.7, 139.0, 137.6, 131.8, 129.9, 128.8, 128.7, 128.4, 128.3, 21.1, 20.9, 20.6, 20.4. HRMS ESI $C_{52}H_{44}N_6O_2Cu^+$ calcd 847.2822 found 847.2817.

*nanoITO nanoparticle films.* Preparation of nanoITO films was by a method similar to that previously reported in the literature.[12] Aldrich Indium tin oxide, dispersion (<100 nm particle size, 30% wt in isopropanol, part 700460) was used. The commercial indium tin oxide dispersion was sonicated and vigorously stirred. A 10 wt% solution of hydroxypropyl cellulouse in ethanol was prepared. A 1:1 v/v mixture of the commercial indium tin oxide dispersion and the hydroxypropyl cellulose solution was prepared by stirring overnight. This was doctor bladed on conductive FTO glass (TEC15) (one 3M Scotch Magic Tape thickness), and allowed to dry. The films were heated in a GSL-1700X tube furnace with a two hour ramp from ambient temperature to 500 °C, held at 500 °C for one hour, and allowed to cool from 500 °C to ambient temperature with a 30 minute programmed ramp, the actual cooling process takes significantly longer due to the thermal characteristics of the tube furnace used.

$TiO_2$ particle paste was synthesized based on procedures from the literature.[13, 14] 100 mL water and 0.7 mL 70% $HNO_3$ were added to a flask and stirred vigorously while 17 mL $Ti(O^iPr)_4$ was added dropwise over 20 minutes. The mixture was heated in a metal bead bath set to >100 °until the volume was concentrated to approximately 30 mL. The reaction was transferred to an acid digestion vessel and heated to 200 °C for 10 hours. Some water was lost during this process, likely during cooling so water was added to achieve a total volume of 30 mL and 1.68 g polyethyleneglycol bisphenol A, epichlorohydrin copolymer (15,000-20,000 Da) was dissolved in the suspension.

$TiO_2$ films were prepared by doctor blading the $TiO_2$ particle paste on FTO glass (TEC 15) (one 3M Scotch Magic Tape thickness). After drying, the films were heated in a GSL-1700X tube furnace with a 30 minute ramp from ambient temperature to 450 °C, held at 450 °C for 30 minutes, and allowed to cool from 450 °C to ambient temperature with a 30 minute programmed ramp, the actual cooling process takes significantly longer due to the thermal characteristics of the tube furnace used.

*Immobilization procedure.* Copper(I) complexes were immobilized on *nano*ITO, $TiO_2$, or AAO substrates by soaking the substrate in a ~ 10 mM $CH_2Cl_2$ solution of **1**, **2**, or **3** overnight. They were then rinsed with neat $CH_2Cl_2$ and soaked for an hour in neat $CH_2Cl_2$ to remove any weakly bound Copper(I) complex. Copper(II) samples for EPR were prepared by oxidizing Copper(I) prepared as above in a 100 mM solution of $AgNO_3$ in acetonitrile overnight. The samples were subsequently washed with acetonitrile and soaked in acetonitrile for 1 hour to remove any residual $Ag^+$.

**NMR of intermediates and complexes.**

$^{1}$H NMR, 2,9-dimesityl-1,10-phenanthroline, 500 MHz, $CDCl_3$

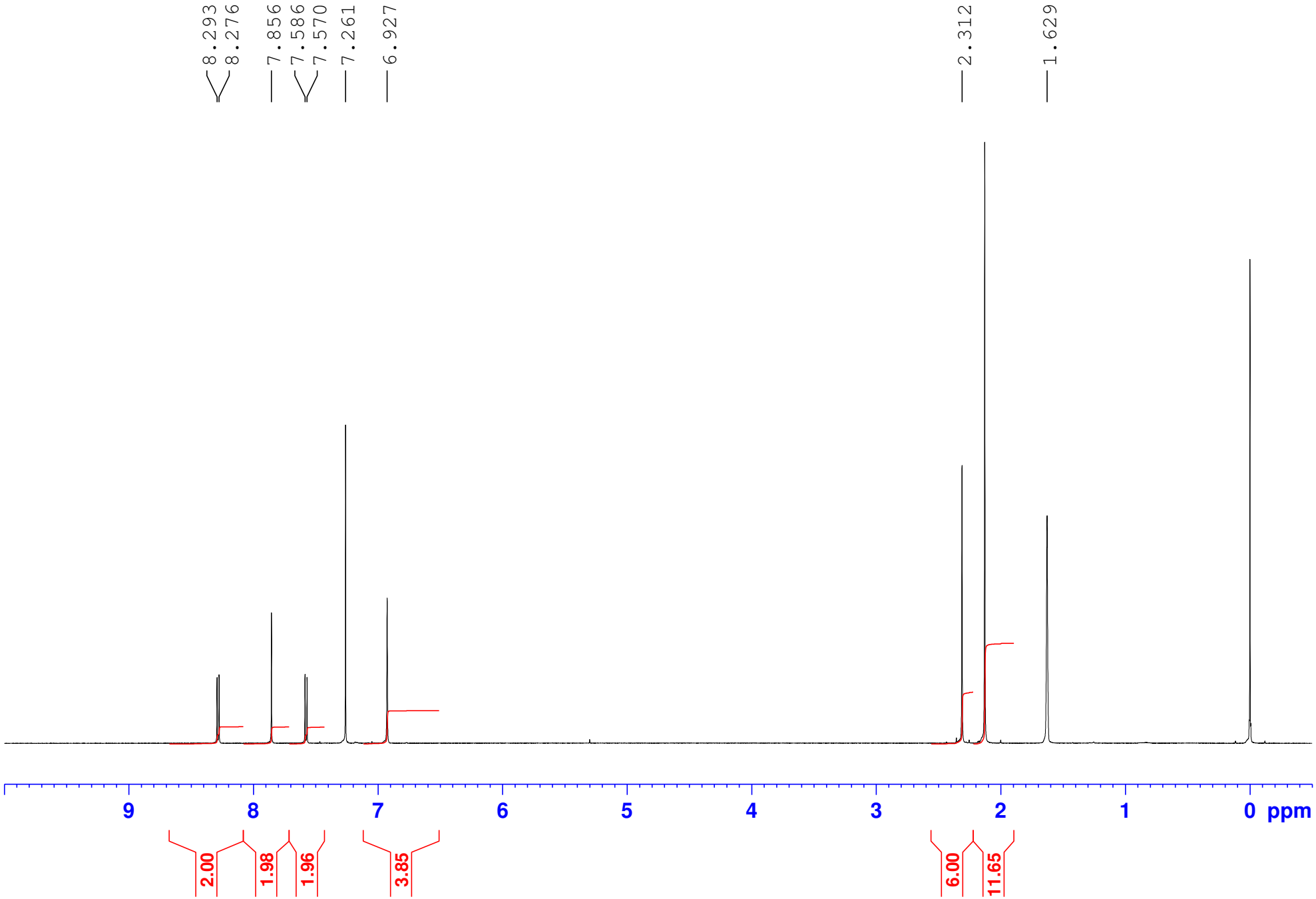

$^{1}$H NMR, 1,10-phenanthroline-4,7-dicarbaldehyde, 500 MHz, DMSO-$d_6$

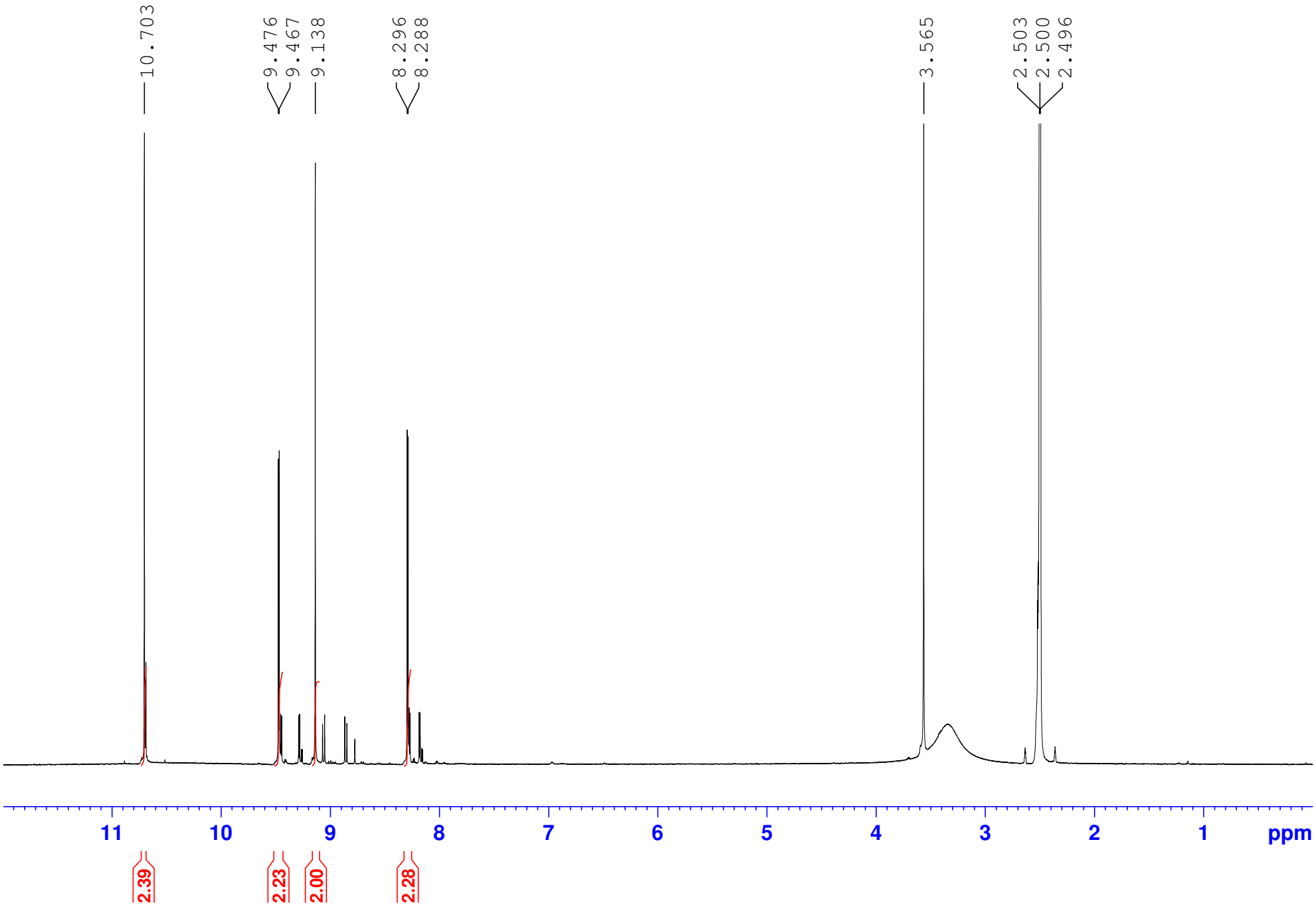

$^{1}$H NMR, 1,10-phenanthroline-4,7-dicarboxylic acid (**L1**), 500 MHz, $D_2O$/NaOD

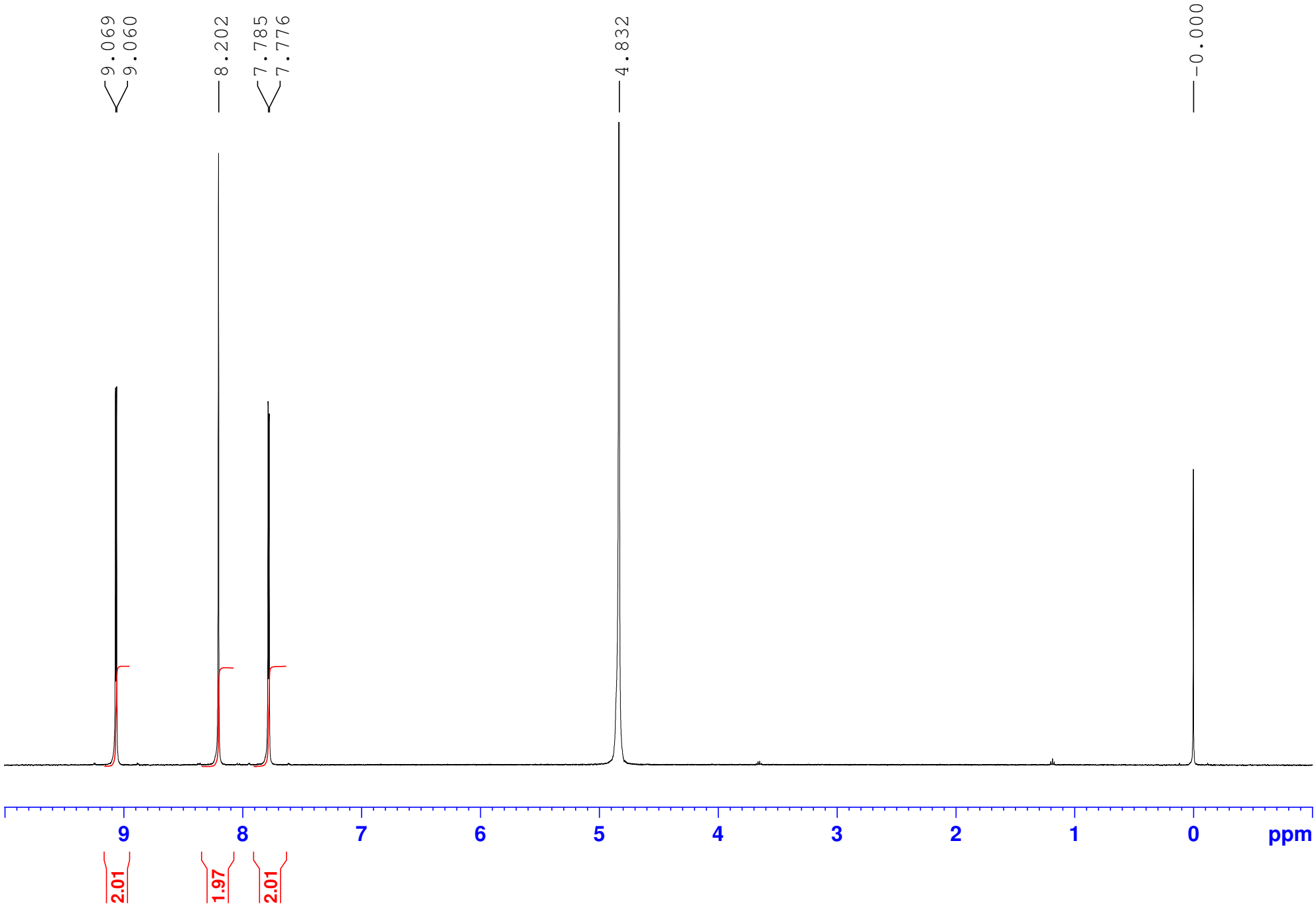

$^{1}$H NMR, **1**, 500 MHz, methanol-$d_4$

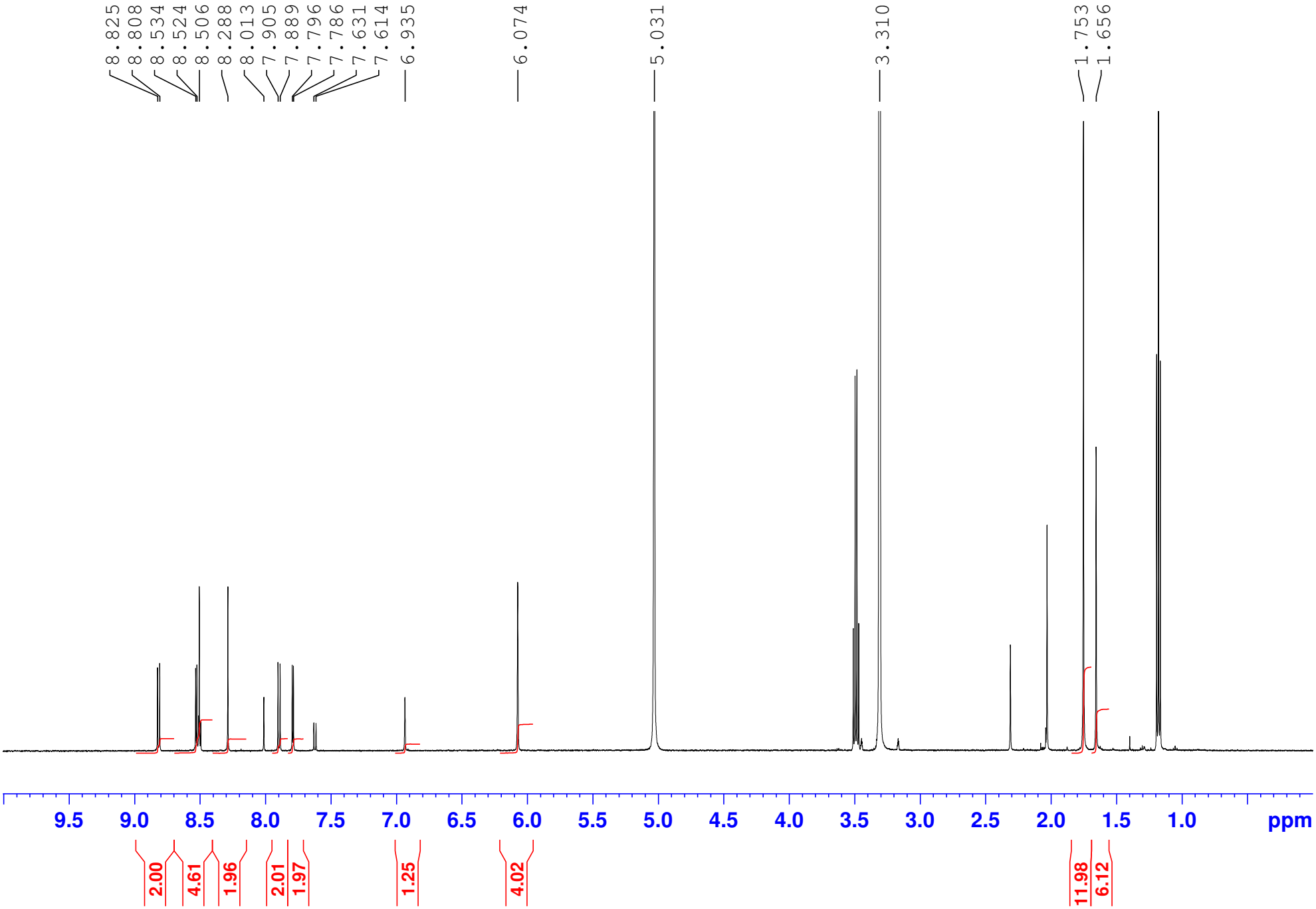

$^{1}$H NMR, **L2**, 500 MHz, DMSO-$d_6$

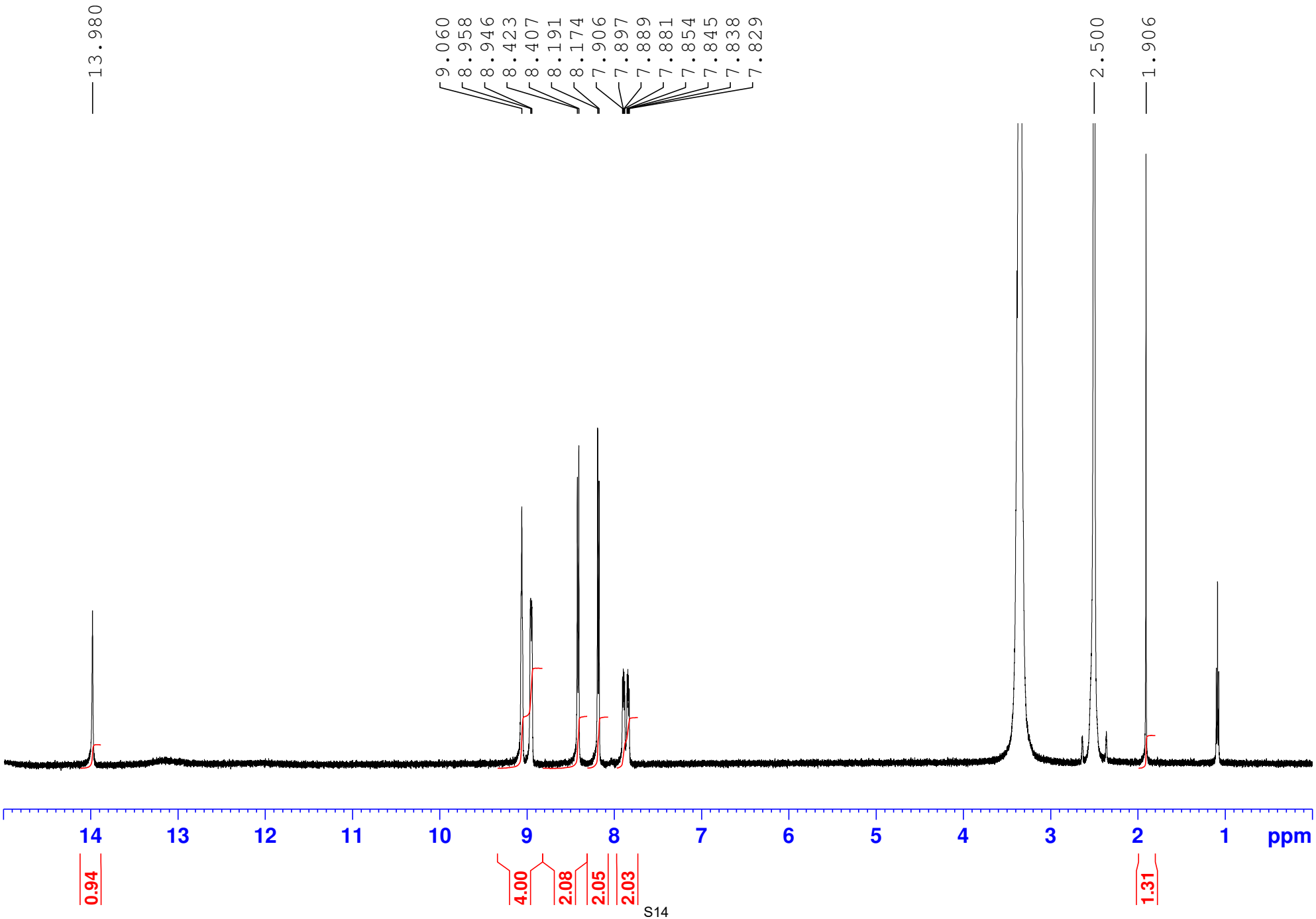

$^{13}$C NMR, **L2**, 125 MHz, DMSO-$d_6$

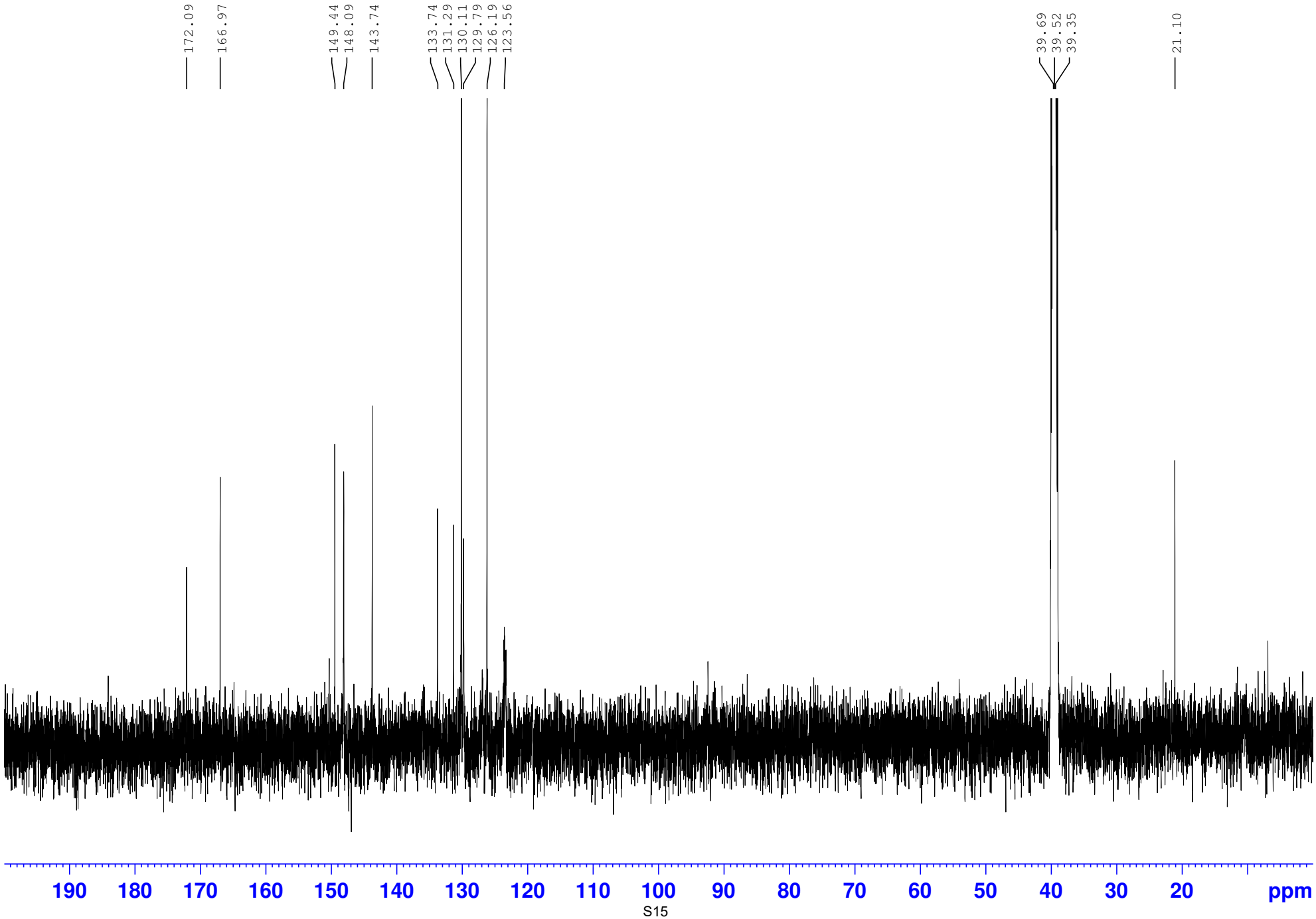

$^{1}$H NMR, **2**, 500 MHz, DMSO-$d_6$

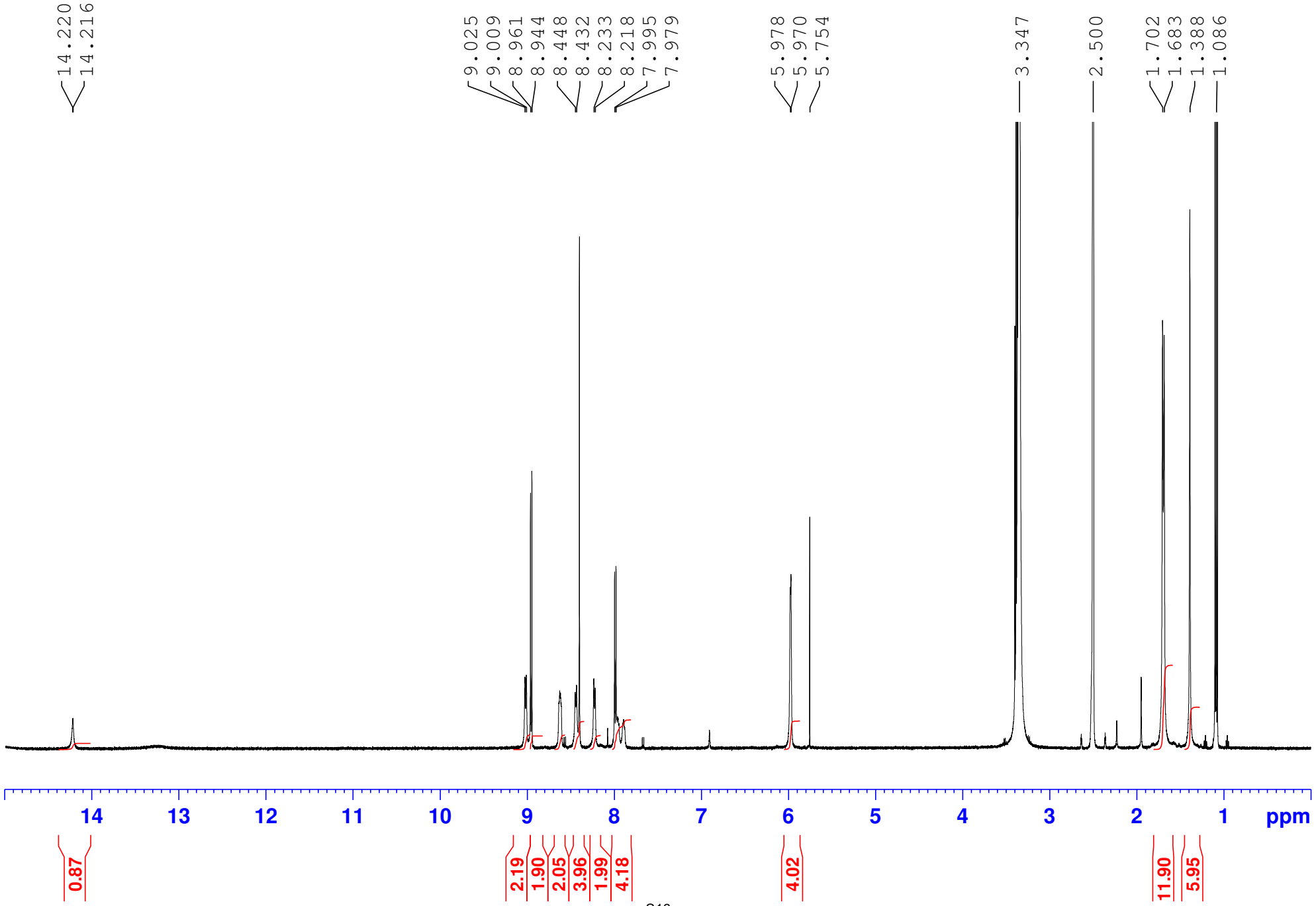

$^{13}$C NMR, **2**, 125 MHz, MeOD

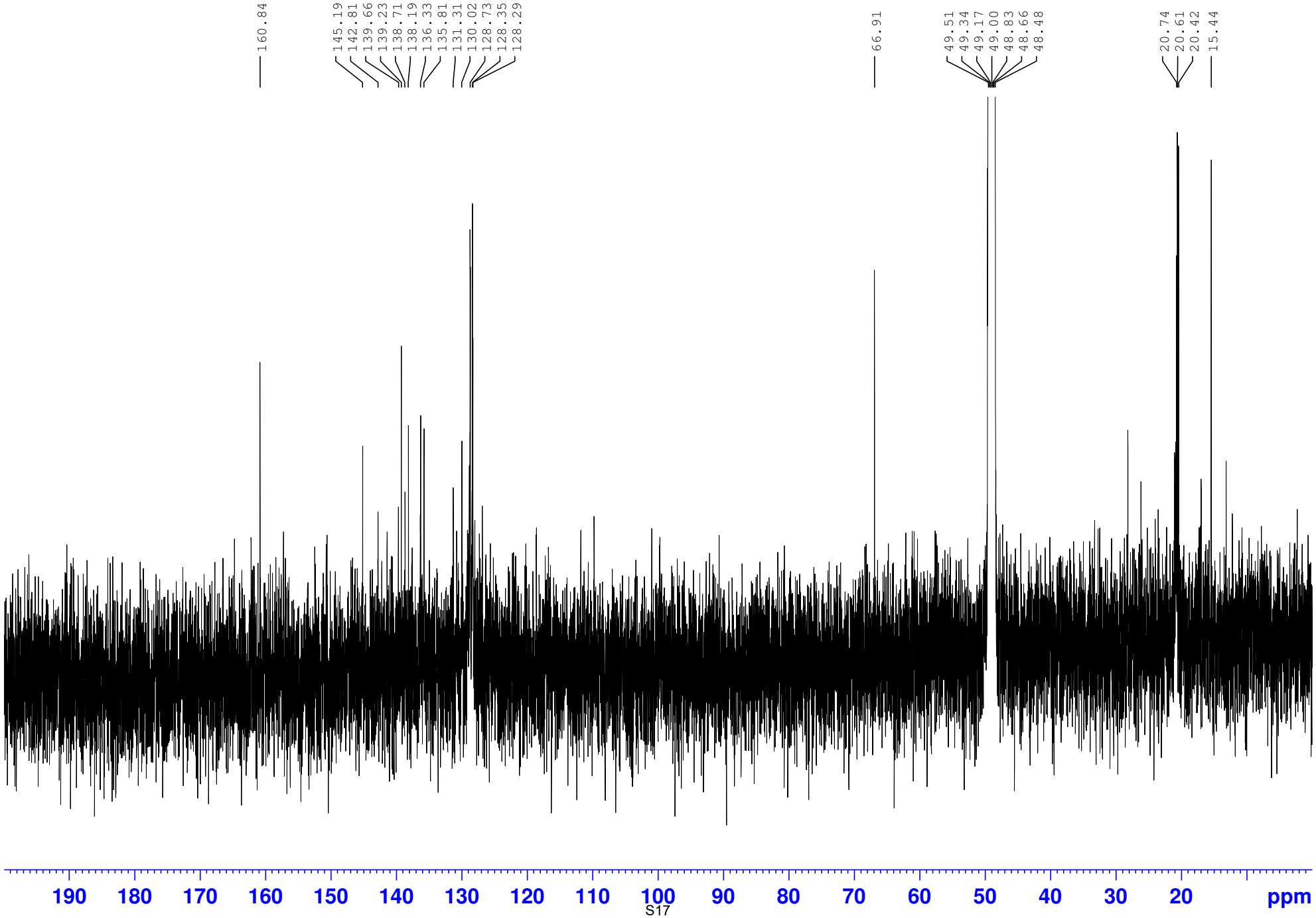

$^{1}$H NMR, 2,9-dimethyl-1,10-phenanthroline-5,6-dione, 500 MHz, $CDCl_3$

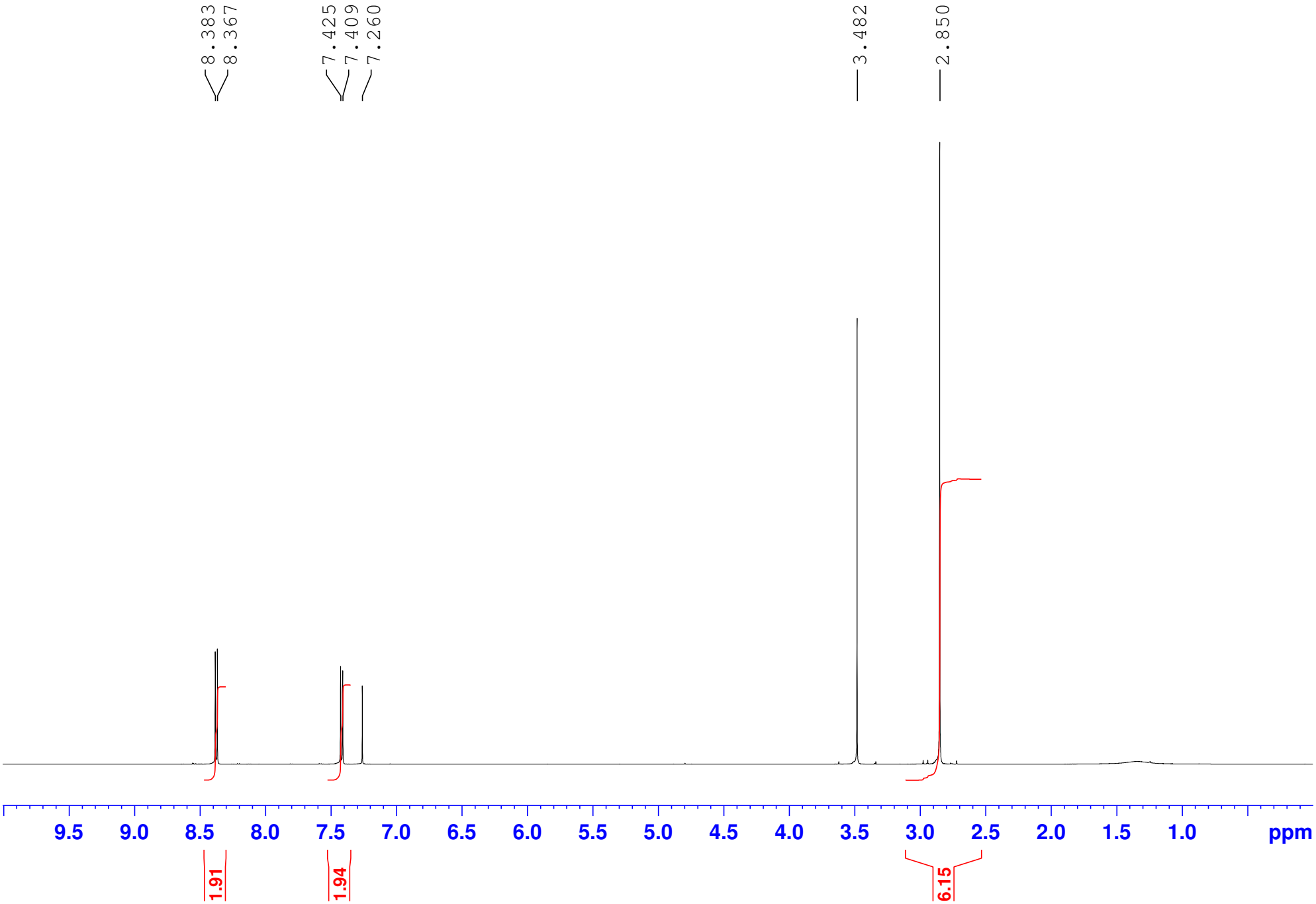

$^{1}$H NMR, **L3**, 500 MHz, MeOD/NaOD

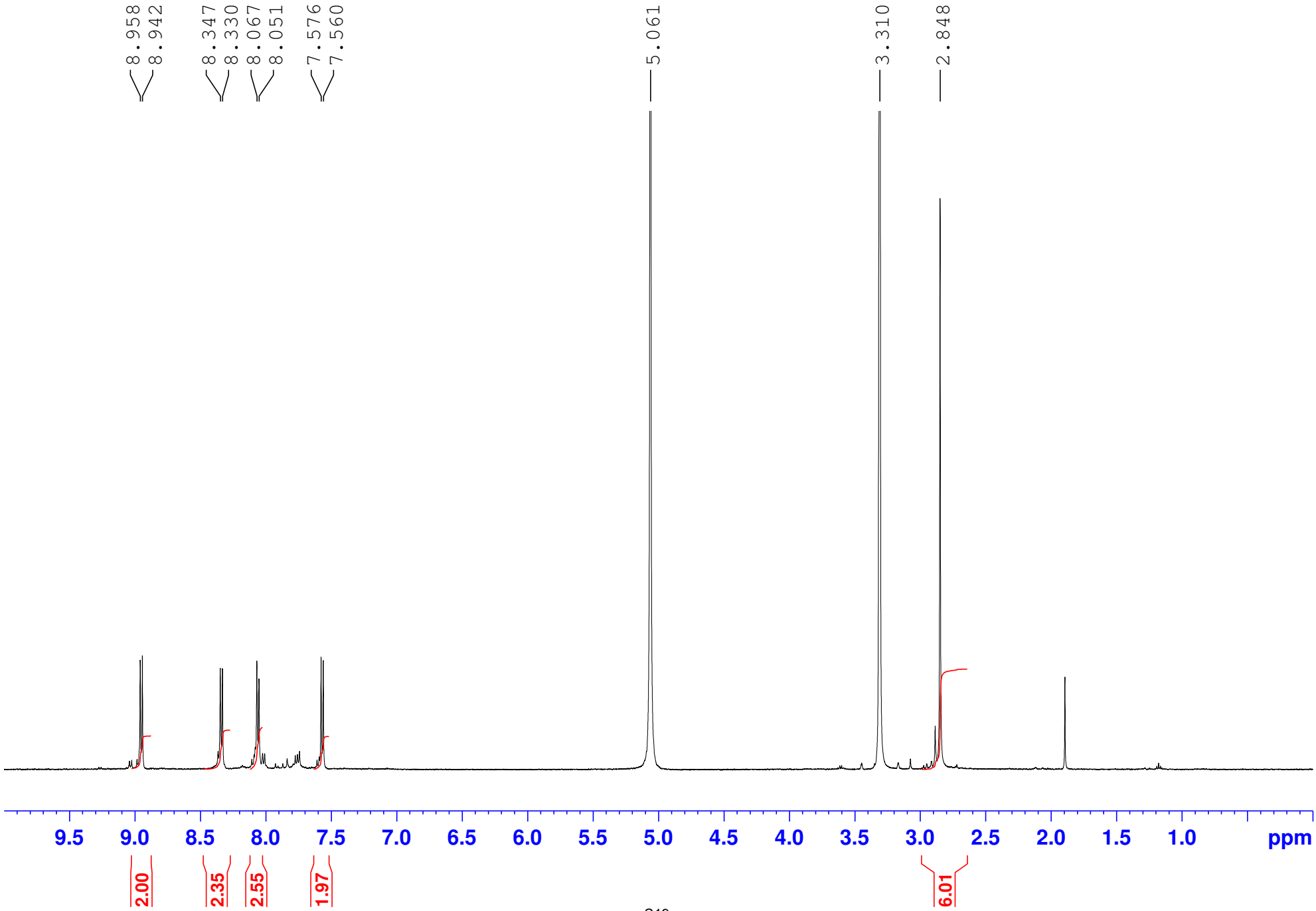

$^{13}$C NMR, **L3**, 125 MHz, DMSO-$d_6$

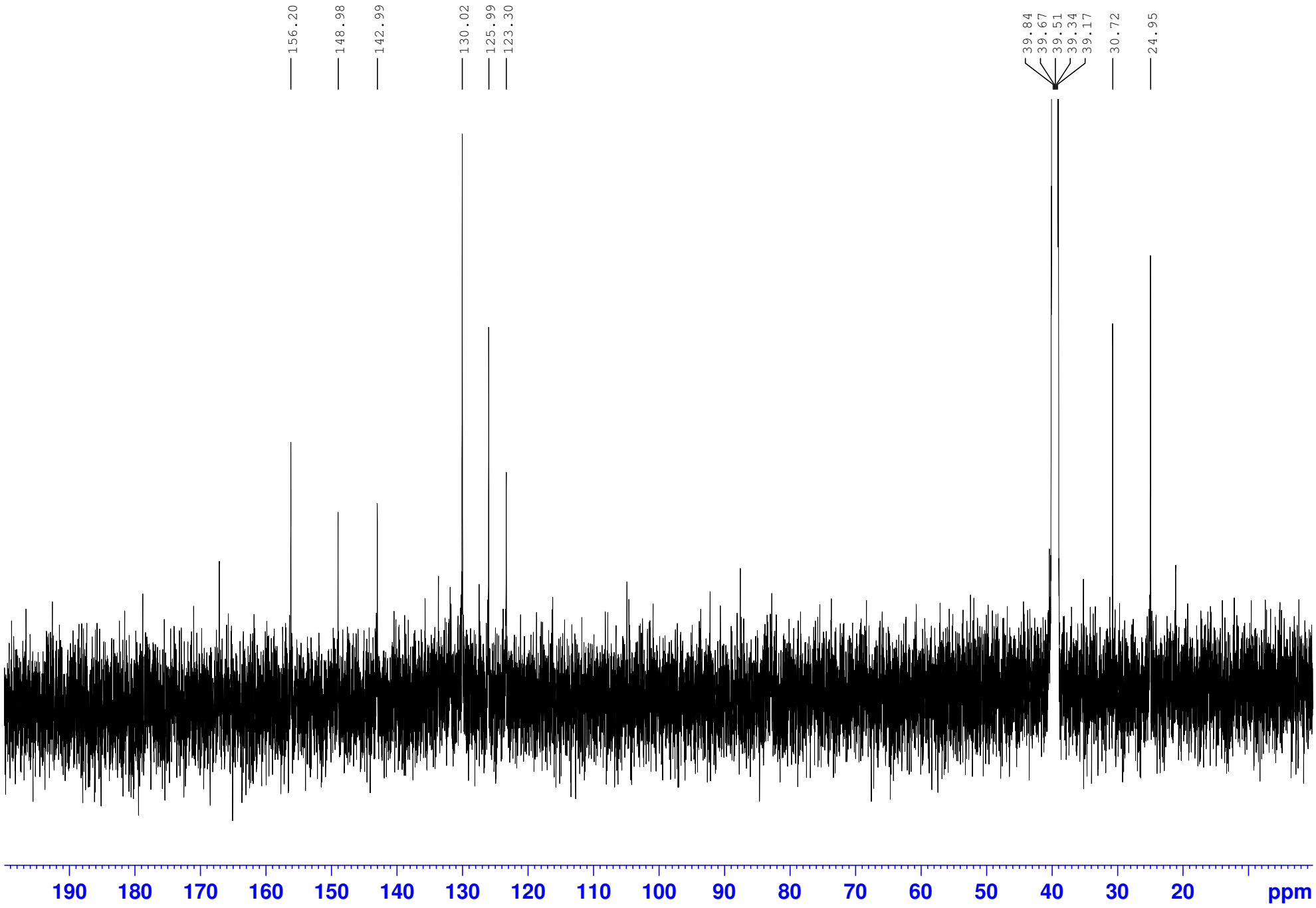

$^{1}$H NMR, **3**, 500 MHz, MeOD

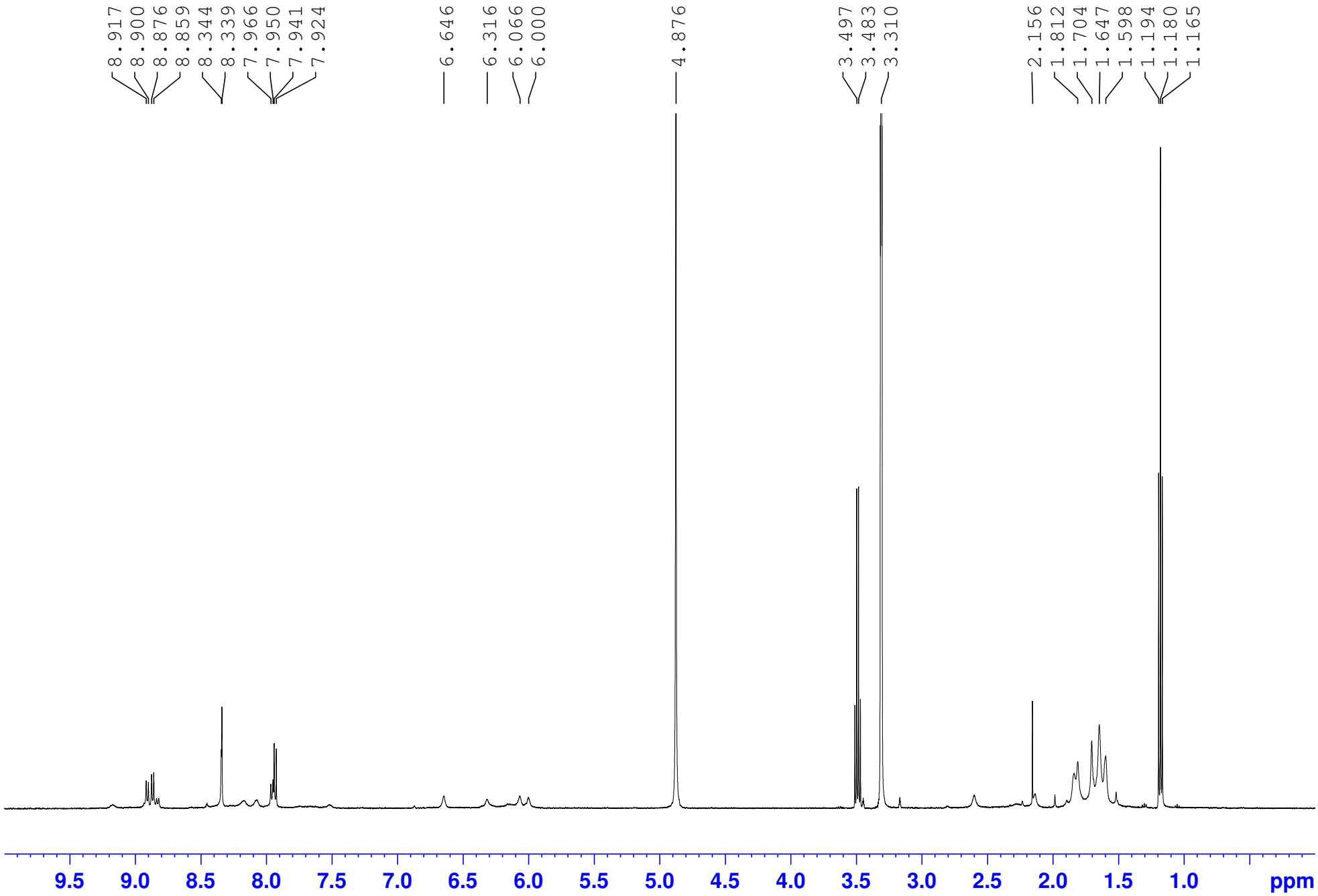

$^{13}$C NMR, **3**, 125 MHz, MeOD

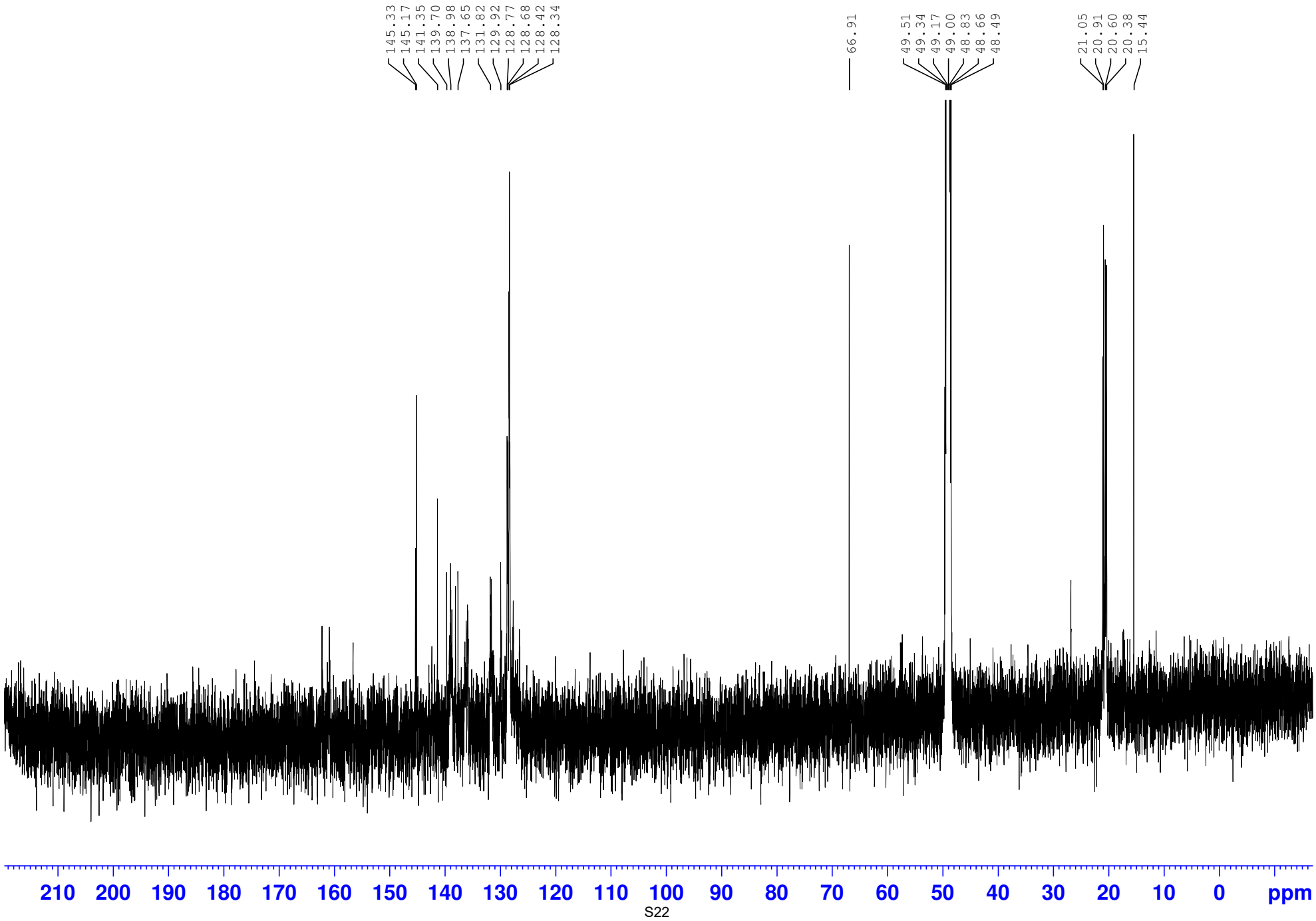

**Energy minimized models of complexes 1 and 3.**

Molecular Mechanics Calculations were performed using Avogadro 1.2.0 and optimized using a UFF force field. The crystallographic coordinates of (phenanthroline)(2,9-dimesityl-1,10-phenanthroline)Copper(I)[5] were used as a starting point for the structures.

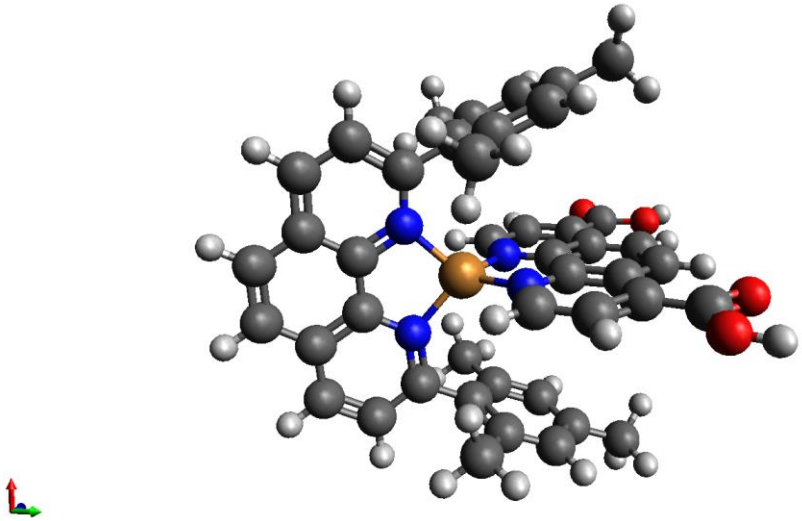

**Figure S1.** Molecular Mechanics Optimized Geometry of **1**.

**Table S1.** Molecular Mechanics Optimized Coordinates of **1**.

| | | | |
|---|---|---|---|
| Cu | -4.18238 | 3.57835 | 3.31528 |
| C | -3.41921 | 4.91077 | 7.71914 |
| C | -3.36468 | 3.52060 | 7.45289 |
| C | -3.57990 | 3.02715 | 6.17106 |
| N | -3.84763 | 3.88974 | 5.17029 |
| C | -3.90908 | 5.23825 | 5.34571 |
| C | -3.70014 | 5.80055 | 6.62518 |
| C | -4.18524 | 6.05638 | 4.21414 |
| C | -4.26626 | 7.46143 | 4.32782 |
| C | -4.05924 | 8.01261 | 5.61131 |
| C | -3.78384 | 7.20684 | 6.72530 |
| N | -4.36976 | 5.45432 | 3.00690 |
| C | -4.64081 | 6.13694 | 1.87584 |
| C | -4.73421 | 7.52367 | 1.92541 |
| C | -4.55074 | 8.22190 | 3.14194 |
| C | -1.53910 | 2.61114 | 2.28469 |
| C | -0.84305 | 1.65118 | 1.53180 |
| C | -1.55735 | 0.62684 | 0.88420 |
| C | -2.95732 | 0.56026 | 0.99975 |
| C | -3.60591 | 1.53350 | 1.77272 |
| N | -2.88842 | 2.51851 | 2.37731 |
| C | -3.72487 | -0.44071 | 0.37582 |
| C | -5.12585 | -0.46276 | 0.52391 |
| C | -5.77629 | 0.51156 | 1.30379 |
| C | -5.01086 | 1.50391 | 1.93215 |
| C | -7.17138 | 0.53792 | 1.47740 |
| C | -7.76633 | 1.54035 | 2.26442 |
| C | -6.95636 | 2.50439 | 2.88666 |
| N | -5.61349 | 2.45190 | 2.70001 |

| | | | |
|---|---|---|---|
| C | -7.51888 | 3.58722 | 3.71511 |
| C | -0.84824 | 3.70614 | 2.98987 |
| C | -0.27957 | 3.50043 | 4.27163 |
| C | 0.32629 | 4.57608 | 4.93713 |
| C | 0.37490 | 5.84725 | 4.35281 |
| C | -0.17791 | 6.04559 | 3.08386 |
| C | -0.78635 | 4.98727 | 2.39331 |
| C | -8.05928 | 4.74342 | 3.10565 |
| C | -8.52887 | 5.79326 | 3.91018 |
| C | -8.46987 | 5.70601 | 5.30683 |
| C | -7.94773 | 4.55494 | 5.90647 |
| C | -7.47424 | 3.49118 | 5.12447 |
| C | -6.94872 | 2.25187 | 5.80013 |
| C | -8.96414 | 6.83087 | 6.16809 |
| C | -8.12593 | 4.87539 | 1.60595 |
| C | -0.30302 | 2.16645 | 4.97509 |
| C | 1.01552 | 6.99851 | 5.07076 |
| C | -1.34744 | 5.23079 | 1.01615 |
| H | -3.15337 | 2.80434 | 8.23687 |
| H | -4.95211 | 8.04600 | 1.00269 |
| H | 0.23509 | 1.69828 | 1.44399 |
| H | -1.01897 | -0.10898 | 0.29960 |
| H | -3.24433 | -1.20176 | -0.22675 |
| H | -5.69794 | -1.23914 | 0.03078 |
| H | -7.79791 | -0.20789 | 1.00381 |
| H | -8.84141 | 1.56163 | 2.39130 |
| H | 0.75611 | 4.42068 | 5.92007 |
| H | -0.12939 | 7.03018 | 2.63330 |
| H | -8.93666 | 6.68446 | 3.44814 |
| H | -7.91481 | 4.48923 | 6.98782 |
| H | -6.96621 | 2.34203 | 6.90705 |
| H | -5.91272 | 2.04873 | 5.47853 |
| H | -7.57643 | 1.38228 | 5.51306 |
| H | -9.35033 | 7.67523 | 5.55836 |
| H | -8.13285 | 7.20774 | 6.80073 |
| H | -9.78388 | 6.46751 | 6.82297 |
| H | -8.75859 | 4.06601 | 1.18593 |
| H | -7.10810 | 4.79852 | 1.17348 |
| H | -8.56183 | 5.84850 | 1.29501 |
| H | -0.81242 | 1.37233 | 4.39439 |
| H | -0.82941 | 2.26714 | 5.94664 |
| H | 0.73825 | 1.83310 | 5.16834 |
| H | 1.41006 | 6.69430 | 6.06358 |
| H | 0.26686 | 7.80436 | 5.22379 |
| H | 1.85765 | 7.39446 | 4.46503 |
| H | -1.23078 | 6.28931 | 0.70050 |
| H | -2.42146 | 4.97319 | 0.98879 |
| H | -4.09881 | 9.06742 | 5.80613 |
| H | -3.64331 | 7.73643 | 7.64604 |
| C | -3.17079 | 5.33076 | 9.14178 |
| O | -2.93888 | 4.48079 | 9.99077 |
| O | -3.19313 | 6.62098 | 9.52786 |
| H | -3.03202 | 6.88114 | 10.44615 |
| C | -4.67382 | 9.71641 | 3.07807 |
| O | -4.53589 | 10.41874 | 4.06478 |
| O | -4.94592 | 10.31588 | 1.89705 |

| | | | |
|---|---|---|---|
| H | -5.03166 | 11.27710 | 1.82252 |
| H | -3.53231 | 1.96436 | 5.97412 |
| H | -4.78415 | 5.60838 | 0.94311 |
| H | -0.81544 | 4.59003 | 0.28198 |

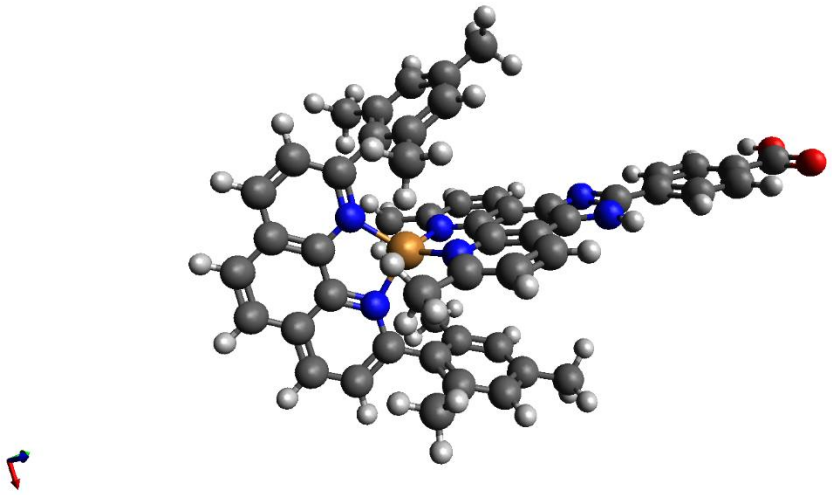

**Figure S2.** Molecular Mechanics Optimized Geometry of **3**.

**Table S2.** Molecular Mechanics Optimized Coordinates of **3**.

| | | | |
|---|---|---|---|
| Cu | -6.50741 | 2.15732 | 3.82457 |
| C | -5.40168 | 3.63773 | 8.10878 |
| C | -5.30965 | 2.24954 | 7.92724 |
| C | -5.62476 | 1.68052 | 6.67999 |
| N | -6.01597 | 2.50123 | 5.66503 |
| C | -6.10300 | 3.85286 | 5.80365 |
| C | -5.79969 | 4.45679 | 7.04182 |
| C | -6.49933 | 4.64649 | 4.68401 |
| C | -6.60466 | 6.04697 | 4.79764 |
| C | -6.30306 | 6.61431 | 6.04159 |
| C | -5.91558 | 5.85397 | 7.11717 |
| N | -6.76931 | 4.03936 | 3.49596 |
| C | -7.15461 | 4.72902 | 2.38692 |
| C | -7.27831 | 6.12842 | 2.46767 |
| C | -6.99977 | 6.78753 | 3.67504 |
| C | -3.81918 | 1.08239 | 2.90638 |
| C | -3.14348 | 0.08182 | 2.18939 |
| C | -3.87139 | -0.90173 | 1.50899 |
| C | -5.27252 | -0.90655 | 1.56469 |
| C | -5.92265 | 0.09593 | 2.30646 |
| N | -5.18893 | 1.06356 | 2.93060 |
| C | -6.03345 | -1.88849 | 0.91105 |
| C | -7.43301 | -1.87583 | 0.99539 |
| C | -8.09352 | -0.88768 | 1.74389 |
| C | -7.34501 | 0.09702 | 2.41273 |
| C | -9.48919 | -0.85170 | 1.83939 |
| C | -10.11722 | 0.15313 | 2.58118 |
| C | -9.35067 | 1.11994 | 3.25414 |
| N | -7.97871 | 1.05369 | 3.15993 |
| C | -10.02519 | 2.21594 | 4.01472 |

| | | | |
|---|---|---|---|
| C | -3.05581 | 2.10582 | 3.67142 |
| C | -2.27361 | 1.74744 | 4.80571 |
| C | -1.60730 | 2.74655 | 5.53208 |
| C | -1.69028 | 4.08974 | 5.15431 |
| C | -2.42798 | 4.44037 | 4.02288 |
| C | -3.09864 | 3.46366 | 3.27331 |
| C | -10.90706 | 3.13455 | 3.37111 |
| C | -11.46243 | 4.19444 | 4.10932 |
| C | -11.18191 | 4.35245 | 5.46912 |
| C | -10.35687 | 3.42972 | 6.11113 |
| C | -9.78998 | 2.36111 | 5.40353 |
| C | -8.99715 | 1.34021 | 6.15834 |
| C | -11.77512 | 5.48759 | 6.25155 |
| C | -11.26827 | 3.03647 | 1.90664 |
| C | -2.12288 | 0.33234 | 5.30662 |
| C | -0.98346 | 5.15544 | 5.93939 |
| C | -3.80621 | 3.87535 | 2.01839 |
| N | -6.32999 | 7.91296 | 6.38874 |
| C | -5.95076 | 7.91563 | 7.69375 |
| N | -5.69112 | 6.66638 | 8.16200 |
| C | -5.84034 | 9.16061 | 8.49622 |
| C | -5.44542 | 9.13527 | 9.84437 |
| C | -5.34881 | 10.31974 | 10.57977 |
| C | -5.64346 | 11.56440 | 9.99159 |
| C | -6.03890 | 11.58605 | 8.64023 |
| C | -6.13515 | 10.40057 | 7.90563 |
| C | -5.52974 | 12.81230 | 10.80786 |
| O | -5.18200 | 12.73553 | 11.97630 |
| O | -5.79746 | 14.04045 | 10.30724 |
| C | -7.44969 | 3.99620 | 1.11193 |
| C | -5.51962 | 0.19882 | 6.45885 |
| H | -5.15691 | 4.05950 | 9.07441 |
| H | -4.99437 | 1.62603 | 8.75438 |
| H | -7.58485 | 6.70638 | 1.60496 |
| H | -7.09316 | 7.86509 | 3.72902 |
| H | -2.06102 | 0.06585 | 2.15666 |
| H | -3.33973 | -1.66505 | 0.95381 |
| H | -5.54660 | -2.66573 | 0.33435 |
| H | -7.99883 | -2.64122 | 0.47790 |
| H | -10.09523 | -1.59404 | 1.33402 |
| H | -11.19713 | 0.16298 | 2.64008 |
| H | -1.02365 | 2.47271 | 6.40374 |
| H | -2.46569 | 5.48001 | 3.71829 |
| H | -12.11970 | 4.90515 | 3.62227 |
| H | -10.17113 | 3.53764 | 7.17371 |
| H | -8.87166 | 1.60095 | 7.23091 |
| H | -8.02258 | 1.23450 | 5.69098 |
| H | -9.50906 | 0.35714 | 6.09430 |
| H | -12.41461 | 6.13534 | 5.61492 |
| H | -10.96096 | 6.11083 | 6.67815 |
| H | -12.39718 | 5.08620 | 7.07914 |
| H | -11.81386 | 2.09674 | 1.70062 |
| H | -10.37069 | 3.07694 | 1.26944 |
| H | -11.93640 | 3.86491 | 1.58866 |
| H | -2.68257 | -0.41412 | 4.71377 |
| H | -2.48323 | 0.26997 | 6.35515 |

| | | | |
|---|---|---|---|
| H | -1.05036 | 0.04587 | 5.28354 |
| H | -0.43438 | 4.73025 | 6.80632 |
| H | -1.72457 | 5.88957 | 6.32052 |
| H | -0.25487 | 5.67990 | 5.28591 |
| H | -3.77415 | 4.97305 | 1.85104 |
| H | -4.84357 | 3.54843 | 2.07365 |
| H | -3.33462 | 3.37397 | 1.14730 |
| H | -5.38512 | 6.38397 | 9.11770 |
| H | -5.20798 | 8.20789 | 10.34432 |
| H | -5.04096 | 10.25703 | 11.61619 |
| H | -6.27858 | 12.50602 | 8.13029 |
| H | -6.44273 | 10.45867 | 6.86887 |
| H | -6.07842 | 14.21260 | 9.40107 |
| H | -6.55607 | 3.46485 | 0.73423 |
| H | -7.79824 | 4.68758 | 0.31585 |
| H | -8.22587 | 3.23763 | 1.30024 |
| H | -5.14826 | -0.32101 | 7.36720 |
| H | -4.82453 | -0.00281 | 5.62445 |
| H | -6.49890 | -0.24236 | 6.19515 |

**Calculation of molecular surface coverage by UV-Vis.**

**Table S3.** AAO Surface Area Calculations

| Name | Pore Diameter (nm) | Thickness (µm) | pore density (#/cm$^2$) | macroscopic to nanoscopic surface area ratio (m$^2$/m$^2$) |
|---|---|---|---|---|
| InRedox | 10 | 50 | 1.6 x $10^{11}$ | 2.51 x $10^3$ |
| InRedox | 20 | 50 | 5.0 x $10^{10}$ | 1.57 x $10^3$ |
| InRedox | 40 | 50 | 1.0 x $10^{10}$ | 6.28 x $10^2$ |

**Table S4.** AAO Coverage Calculations

| | Absorbance | ε (cm$^2$/mol) | coverage (mol/cm$^2$) | surface concentration (mol/m$^2$) | area per molecule (nm$^2$) |
|---|---|---|---|---|---|
| 10 nm AAO + **1** | 1.8092 | 4830000 | 3.75 x $10^{-7}$ | 1.49 x $10^{-6}$ | 1.11 |
| 20 nm AAO + **1** | 1.0245 | 4830000 | 2.12 x $10^{-7}$ | 1.35 x $10^{-6}$ | 1.23 |
| 40 nm AAO + **1** | 0.5284 | 4830000 | 1.09 x $10^{-7}$ | 1.74 x $10^{-6}$ | 0.954 |
| 10 nm AAO + **2** | 1.4883 | 7760000 | 1.91 x $10^{-7}$ | 7.63 x $10^{-7}$ | 2.18 |
| 20 nm AAO + **2** | 0.9013 | 7760000 | 1.16 x $10^{-7}$ | 7.40 x $10^{-7}$ | 2.25 |
| 40 nm AAO + **2** | 0.5091 | 7760000 | 6.56 x $10^{-8}$ | 1.04 x $10^{-6}$ | 1.59 |
| 10 nm AAO + **3** | 2.6574 | 5710000 | 4.65 x $10^{-7}$ | 1.82 x $10^{-6}$ | 0.896 |
| 20 nm AAO + **3** | 1.7428 | 5710000 | 3.05 x $10^{-7}$ | 1.94 x $10^{-6}$ | 0.854 |
| 40 nm AAO + **3** | 0.9211 | 5710000 | 1.61 x $10^{-7}$ | 2.57 x $10^{-6}$ | 0.647 |

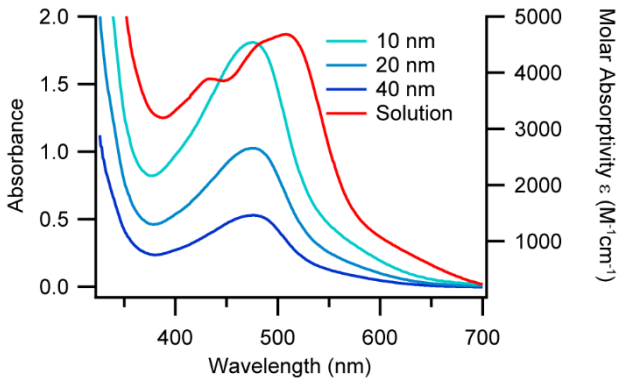


**Figure S3.** Visible absorption spectra of **1** immobilized on AAO (dry) and in homogeneous $CH_2Cl_2$.

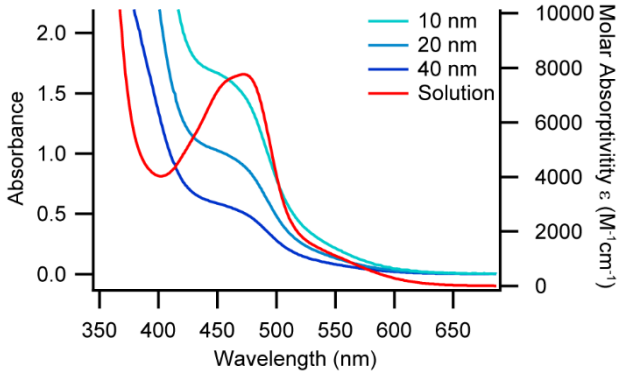


**Figure S4.** Visible absorption spectra of **2** immobilized on AAO (dry) and in homogeneous $CH_2Cl_2$.

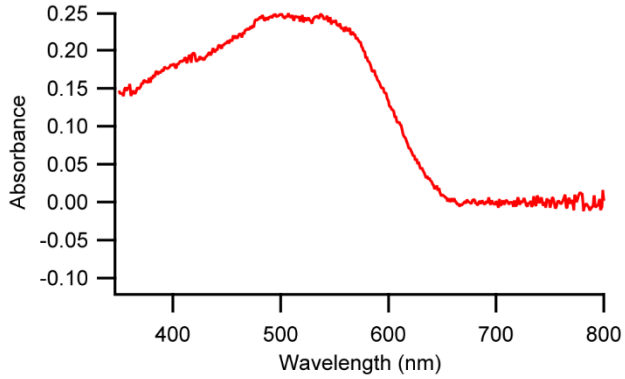


**Figure S5.** Diffuse reflectance spectrum of **2** as a powder.

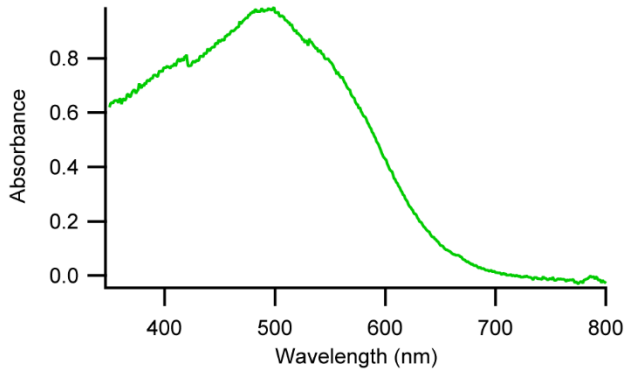


**Figure S6.** Diffuse reflectance spectrum of **3** as a powder.

**Table S5.** Summary of UV-Visible Absorption Properties

| **Complex** | **Solution $\lambda_{max}$** | **Immobilized $\lambda_{max}$** | **ε ($M^{-1}cm^{-1}$)** |
|---|---|---|---|
| **1** | 508 nm, 432 nm | 478 nm | 4800 |
| **2** | 472 nm | - | 7800 |
| **3** | 466 nm | - | 5700 |

**EPR spectra of 3 on AAO and bare AAO.**

For all three AAO pore sizes, we observe spectra characteristic of Cu(II), with S=1/2 ($d^9$ electronic configuration). These spectra are typical for Cu(II) species with axial g-tensor and a resolved parallel component of the $^{63,65}$Cu (I=3/2) hyperfine tensor (A-tensor).[15, 16] No superhyperfine structure from spin-carrying ligand nuclei ($^{14}$N) is visible. The measured magnetic resonance parameters for these spectra are: $g_{II}$=2.26, $g_{per}$=2.07 and $A_{II}$=530 MHz (177*$10^{-4}$ $cm^{-1}$). The strong narrow signal in 40 nm AAO at 338 mT was attributed to an organic radical/defect ($g \approx 2.005$), as it was also observed in the bare AAO lacking any immobilized copper species (Figure S7). The distances between the immobilized Cu(II) complexes were estimated from the broadening of the parallel components of the EPR spectra. Broadening of the line were obtained by comparison with line width (~180 MHz) of the same Cu(II) complexes in diluted glassy frozen solutions, conditions where the electron dipole--dipole interaction is negligible.

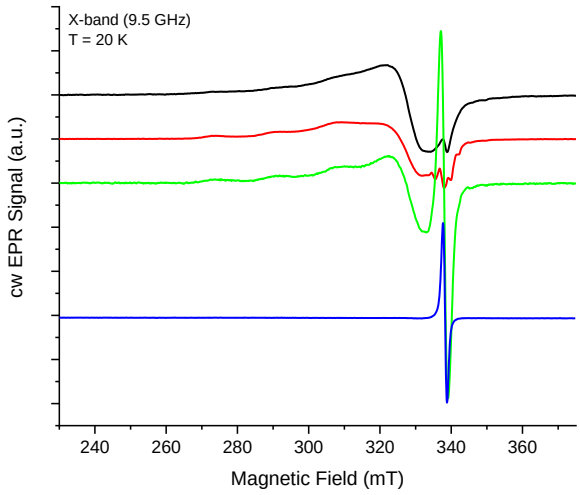


**Figure S7.** CW X-band EPR spectra of oxidized immobilized copper (**3**$^{2+}$) in AAO with 10 nm (black), 20 nm (red), and 40 nm (green) pore size, respectively. An EPR spectrum of neat 40 nm AAO without copper (blue) is shown for comparison. Measurements were conducted at 20 K. Spectra have been scaled for better visibility.

**Cyclic voltammetry of 1-3 in $CH_3CN$ solution.**

The Cu(II/I) couple of **1** shifts 0.23 V more negative when immobilized (-0.09 V vs. $Fc^{+/0}$, see Figure 3 in the main text) as compared to in solution (0.14 V vs $Fc^{+/0}$, Figure S4). An identical shift of 0.23 V more negative is observed for **2** ( +.15 V vs $Fc^{+/0}$ in solution, -0.08 V vs $Fc^{+/0}$ immobilized) This is opposite of what we might expect if the oxidation-induced flattening distortion is restricted on immobilization, but this shift could also be a result of electronic changes in the carboxylic acid functional groups upon surface immobilization. The potential of **3** shifted anodically 0.05 V (0.41 vs $Fc^{+/0}$ in solution, +.36 V vs $Fc^{+/0}$ immobilized)

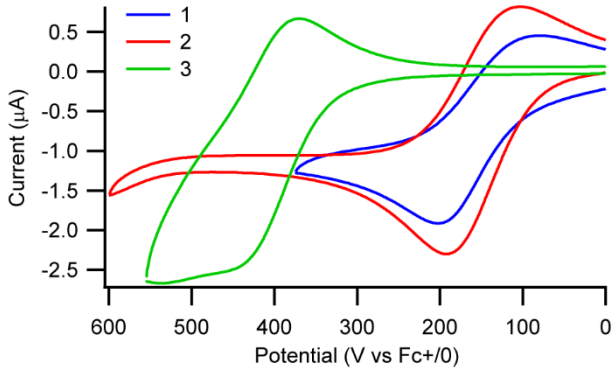


**Figure S8.** Cyclic voltammogram of 1 mM **1-3** in $CH_3CN$ containing 0.1 M $NBu_4PF_6$ with a gold working electrode.

We note that we observe substantially lower peak currents of **1** compared to **2** and **3** despite the identical *nano*ITO substrates used for the CV measurements (Figure 3 in main text). We presume that this is a result of less efficient surface packing than for **2** and **3** as a consequence of the very short anchor length of **1**.

**Table S6.** Summary of Electrochemical Properties

| Complex | Solution $E_{1/2}$ (V vs $Fc^{+/0}$) | Immobilized $E_{1/2}$ (V vs $Fc^{+/0}$) |
|---|---|---|
| **1** | +0.14 | -0.09 |
| **2** | +0.15 | -0.08 |
| **3** | +0.41 | +0.36 |

**Kinetic fitting procedure.**

Kinetic traces at selected probe wavelengths *S(λ,t)* from transient absorption spectra were fit using the product of the Heaviside step function *H(t-t$_0$)* and a sum of exponential functions convoluted with a Gaussian instrument response function (Equation S3) unless otherwise specified. $A_n$ are the amplitudes and $\tau_n$ are the time constants for the exponential functions, $t_0$ is time zero, and *w* is the width of the Gaussian instrument response. Global fitting was accomplished using the Global Fit package in Igor Pro 8.04 by allowing $A_n$, $t_0$, and *w* to vary for each selected wavelength but sharing a common set of $\tau_n$ among all of the selected wavelengths.

$$S(\lambda,t) = \left( H(t-t_0) \times \sum_n A_n e^{-(t-t_0)/\tau_n} \right) * e^{-t^2/2w^2} \quad \text{(S3)}$$

**Transient spectra and kinetic fits for solution and immobilized complexes.**

*Considerations for solution phase data.* Cu(I)bis(phen) complexes are known to undergo three distinct photophysical processes: an initially formed $^1$MLCT state undergoes a rapid flattening distortion on the sub-picosecond timescale followed by relatively slow intersystem crossing to a $^3$MLCT state which then decays back to the ground state. Because of the complex spectral changes and multiple photophysical processes, we used global analysis to fit the transient absorption data over a broad range of wavelengths with Equation S3, assuming first order kinetic processes. The excited-state dynamics in solution are summarized in Table S7; spectra and kinetics are shown in Figures S8-S37. These kinetic parameters reflect intersystem crossing and $^3$MLCT decay.

**Table S7.** Summary of excited-state lifetimes for **1**, **2**, and **3** dissolved in $CH_2Cl_2$ as measured by ultrafast transient optical spectroscopy.

| | **1** | **2** | **3** |
|---|---|---|---|
| $\tau_1$ | 1.2 ps | 5 ps | 4.5 ps |
| $\tau_2$ | 20 ps | 55 ps | 170 ps |
| $\tau_3$ | 1 ns | 2.9 ns | 48.7 ns |

*Considerations for immobilized data.* In this work, the excited-state lifetime increased so that the majority of the excited-state decay does not occur within the three nanosecond window of the femtosecond laser system. To more fully understand kinetics of **3** immobilized on AAO, we investigated them with the nanosecond transient absorption system where decay of the $^3$MLCT was readily fit with Equation S3 using a sum of two exponential functions. We incorporated the lifetime values found from fitting the nanosecond data as fixed parameters along with two additional components to model the sub-nanosecond processes for **3** on AAO. The kinetics are summarized in Table S8. Average lifetimes for $^3$MLCT decay were weighted by spectral mass of the fit components.

**Table S8.** Summary of excited-state lifetimes for **1** and **3** immobilized on AAO and immersed in $CH_2Cl_2$ as measured by nanosecond transient optical spectroscopy.

| | **1** (20 nm) | **3** (10 nm) | **3** (20 nm) | **3** (40 nm) |
|---|---|---|---|---|
| $\tau_1$ | 5.8 ps | 8 ps | 8 ps | 8 ps |
| $\tau_2$ | 95 ps | 240 ps | 140 ps | 160 ps |
| $\tau_3$ | 1.7 ns | 16 ns | 18 ns | 9.6 ns |
| $\tau_4$ | - | 120 ns | 120 ns | 88 ns |
| $\tau_{3,4(avg)}$ | | 69 ns | 69 ns | 51 ns |

**Complex 1 in $CH_2Cl_2$ solution: ultrafast transient absorption.**

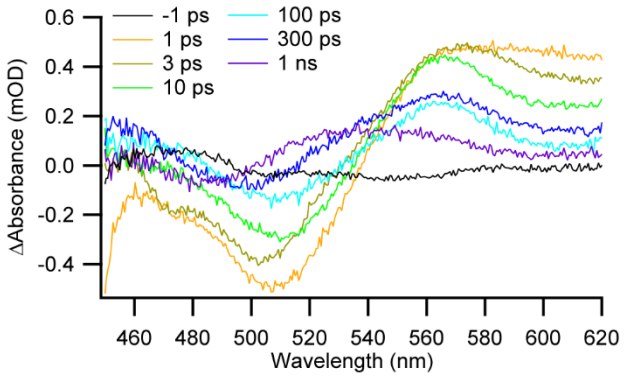


**Figure S8.** Ultrafast transient absorption spectrum for **1** in $CH_2Cl_2$. Time delay noted in legend.

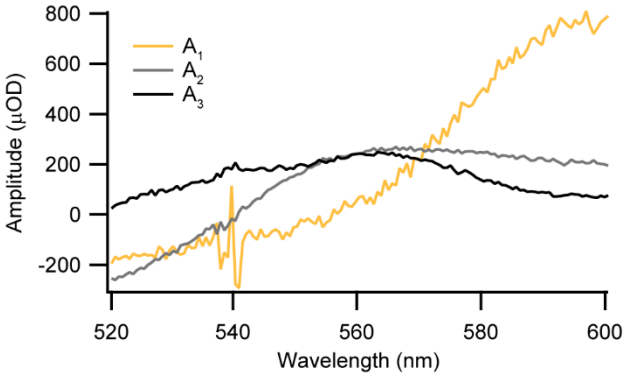


**Figure S9.** Fit parameters for ultrafast transient absorption of **1** in $CH_2Cl_2$.

$\tau_1$ = 1.2 ps
$\tau_2$ = 20 ps
$\tau_3$ = 1.0 ns
fwhm = 120 fs
$A_1$, $A_2$, $A_3$ = shown as a function of wavelength

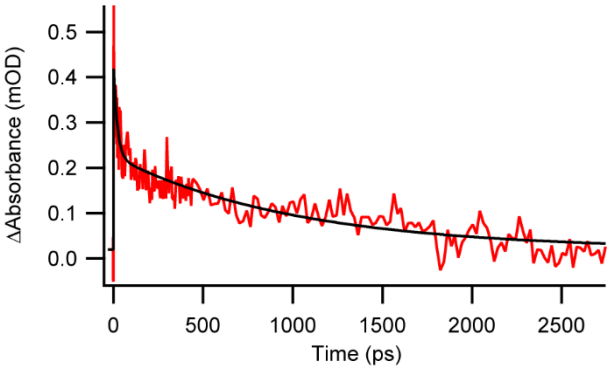


**Figure S10.** Kinetic trace at 555 nm for **1** in $CH_2Cl_2$ Solution.

**Complex 2 in $CH_2Cl_2$ solution: ultrafast transient absorption.**

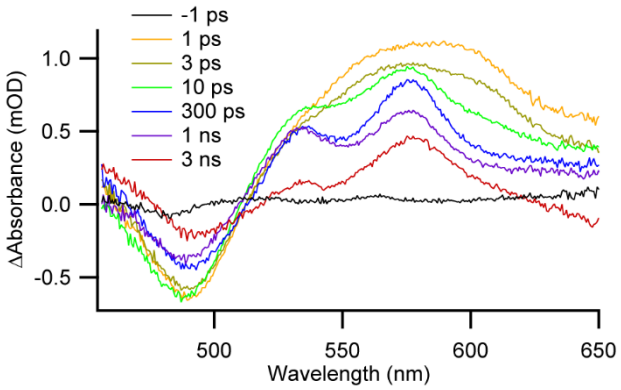


**Figure S11.** Ultrafast transient absorption spectrum for **2** in $CH_2Cl_2$. Time delay noted in legend.

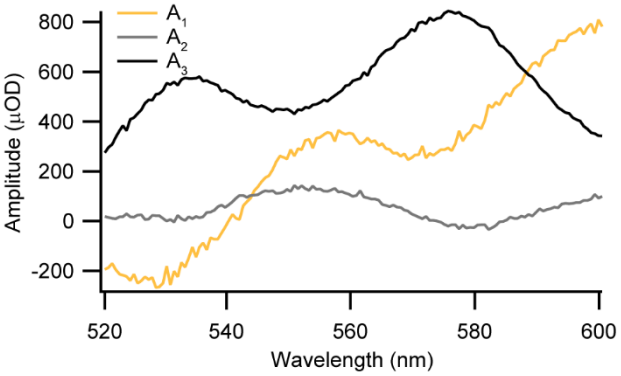


**Figure S12.** Fit parameters for ultrafast transient absorption of **2** in $CH_2Cl_2$ solution.

$\tau_1$ = 5 ps
$\tau_2$ = 55 ps
$\tau_3$ = 2.9 ns
fwhm = 240 fs
$A_1$, $A_2$, $A_3$ = shown as a function of wavelength

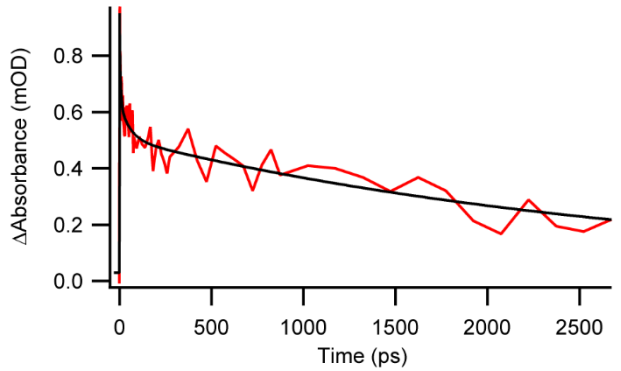


**Figure S13.** Kinetic trace at 555 nm for **2** in $CH_2Cl_2$ solution.

**Complex 3 in $CH_2Cl_2$ solution: ultrafast transient absorption.**

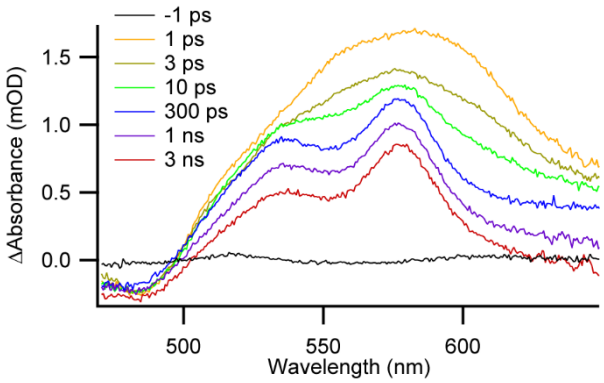


**Figure S14.** Ultrafast transient absorption spectrum for **3** in $CH_2Cl_2$ solution.

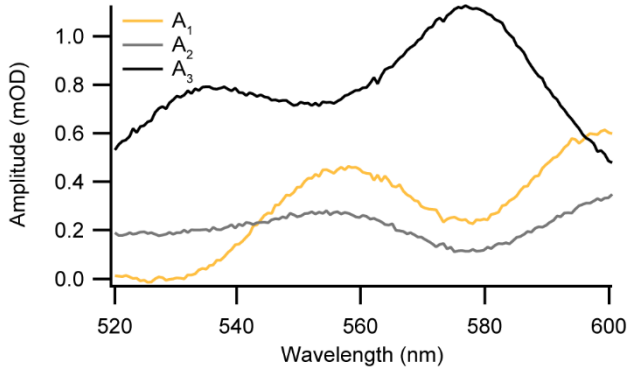


**Figure S15.** Fit parameters for ultrafast transient absorption of **3** in $CH_2Cl_2$ solution.

$\tau_1$ = 4.5 ps
$\tau_2$ = 170 ps
$\tau_3$ = 8.9 ns (reported as > 3 ns)
fwhm = 240 fs
$A_1$, $A_2$, $A_3$ = shown as a function of wavelength

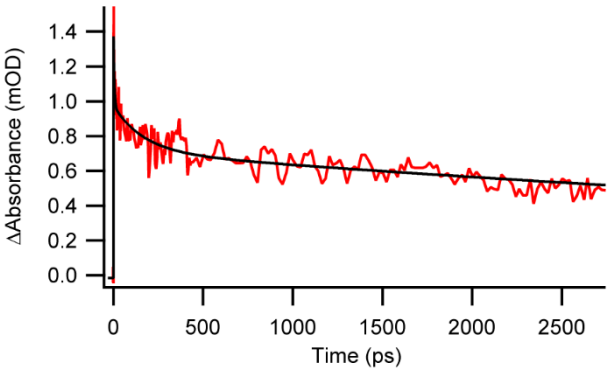


**Figure S16.** Kinetic trace at 555 nm for **3** in $CH_2Cl_2$ solution.

**Complex 3 in $CH_2Cl_2$ solution: nanosecond transient absorption**

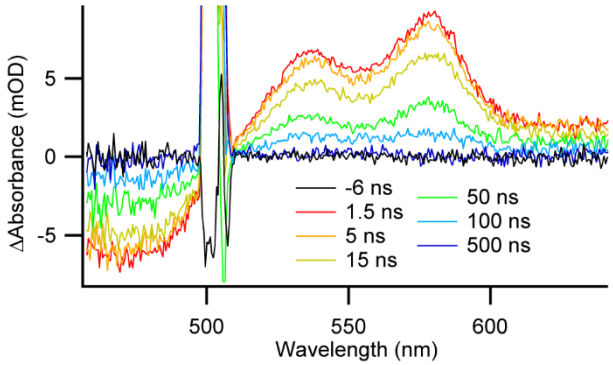


**Figure S17.** Nanosecond transient absorption spectrum for **3** in $CH_2Cl_2$ solution.

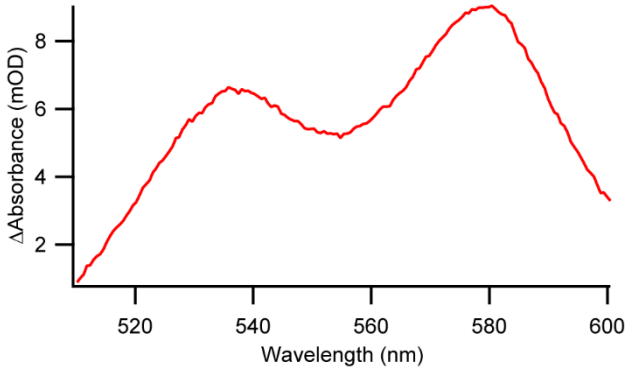


**Figure S18.** Fit parameters for nanosecond transient absorption of **3** in $CH_2Cl_2$ solution.

$\tau_1$ = 48.7 ns
fwhm = 1.0 ns
$A_1$ = shown as a function of wavelength

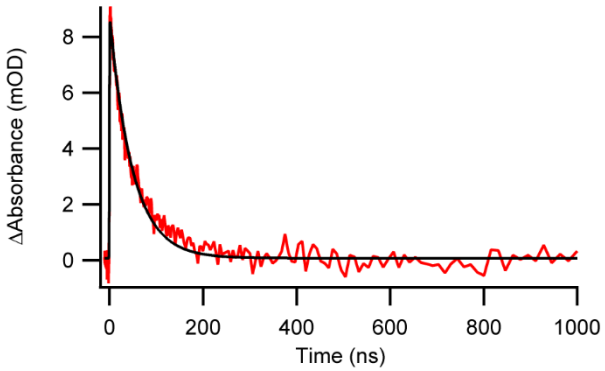


**Figure S19.** Nanosecond kinetic trace at 575 nm for **3** in $CH_2Cl_2$ solution.

**Complex 1 immobilized on 20 nm AAO: ultrafast transient absorption.**

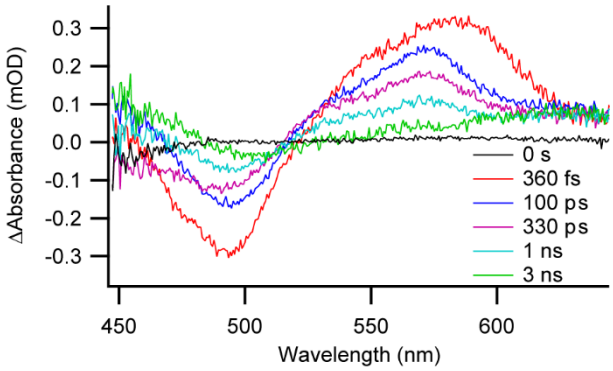


**Figure S20.** Transient absorption spectra of **1** on 20 nm AAO in $CH_2Cl_2$.

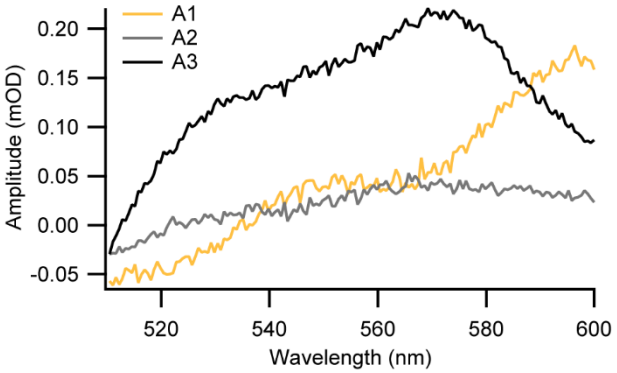


**Figure S21.** Fit parameters for ultrafast transient absorption of **1** on 20 nm AAO.
$\tau_1$ = 5.8 ps
$\tau_2$ = 95 ps
$\tau_3$ = 1.7 ns
fwhm = 240 fs
$A_1$, $A_2$, $A_3$ = shown as a function of wavelength

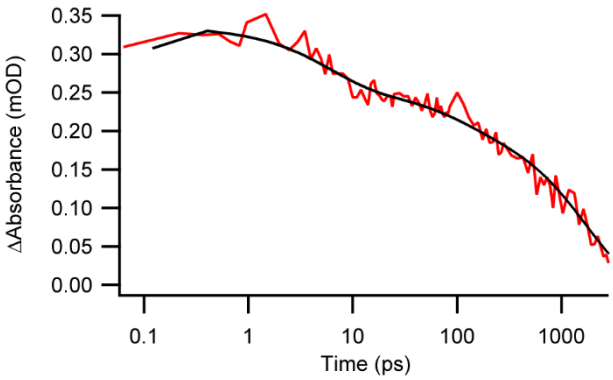


**Figure S22.** Kinetic trace at 575 nm for **1** on 20 nm AAO.

**Complex 3 immobilized on 40 nm AAO: ultrafast transient absorption.**

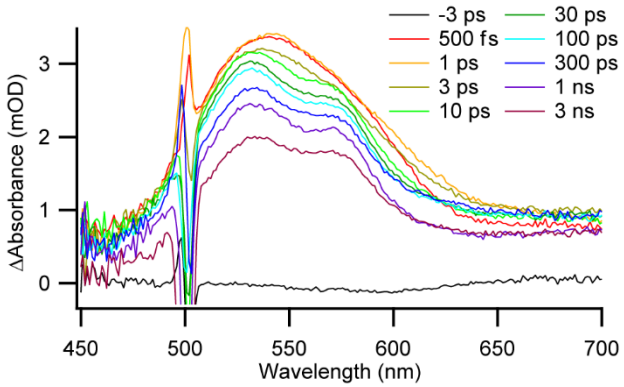


**Figure S23.** Ultrafast transient absorption spectrum for **3** on 40 nm AAO.

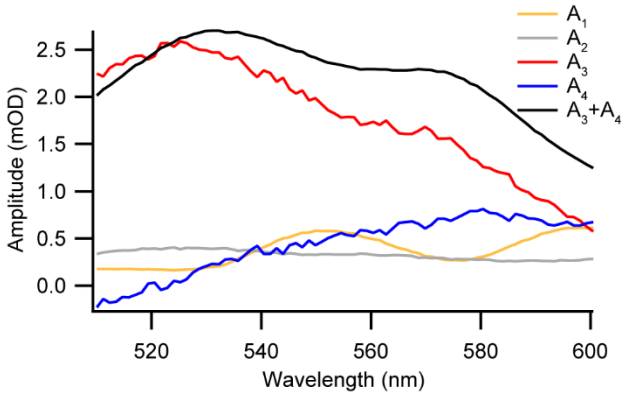


**Figure S24.** Global fit parameters of ultrafast transient absorption for **3** on 40 nm AAO.
$\tau_1$ = 8 ps
$\tau_2$ = 160 ps
$\tau_3$ = 9.6 ns (fixed based on nanosecond data)
$\tau_4$ = 88 ns (fixed based on nanosecond data)
fwhm = 300-400 fs
$A_1$, $A_2$, $A_3$, $A_4$ = shown as a function of wavelength
The lifetimes for the two longer time components were fixed based on nanosecond data. Because their lifetimes are far in excess of the experiment limits, their spectral components show some dependency (observed as equal and opposite apparent noise). Their sum is also shown, which reflects the spectral components observed on a nanosecond transient absorption spectrometer as in Figure S27.

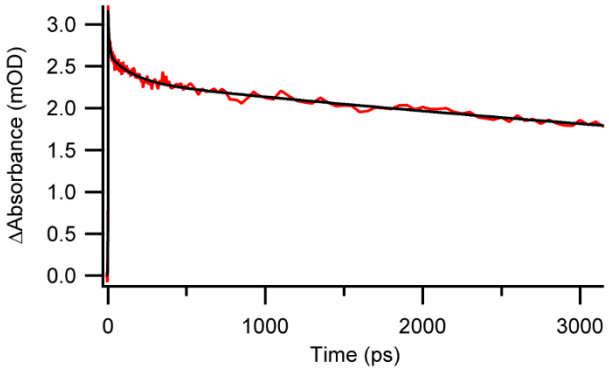


**Figure S25.** Kinetic trace at 555 nm for **3** on 40 nm AAO.

**Complex 3 immobilized on 40 nm AAO: nanosecond transient absorption.**

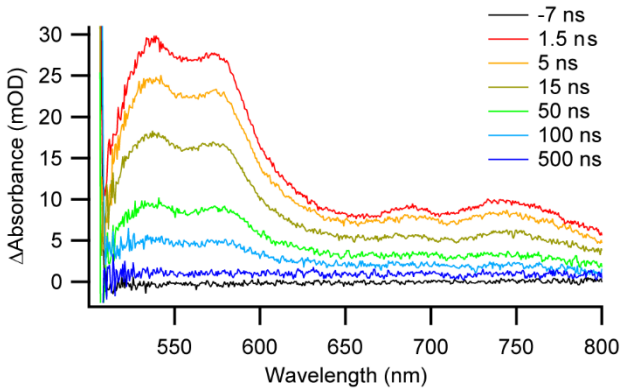


**Figure S26.** Nanosecond transient absorption spectrum for **3** on 40 nm AAO.

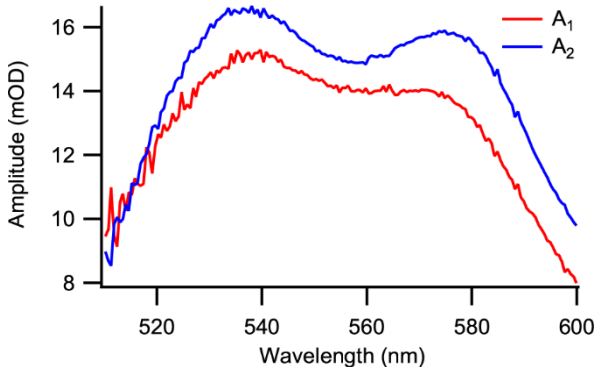


**Figure S27.** Global fit parameters from nanosecond transient absorption of **3** on 40 nm AAO.
$\tau_1$ = 9.6 ns
$\tau_2$ = 88 ns
fwhm = 1.0 ns
$A_1$, $A_2$ = shown as a function of wavelength

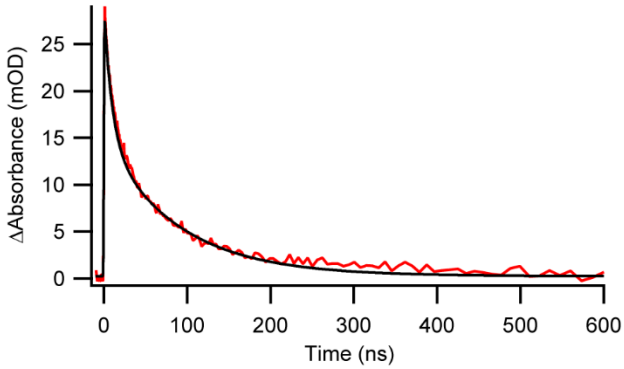


**Figure S28.** Kinetic trace at 575 nm for **3** on 40 nm AAO.

**Complex 3 immobilized on 20 nm AAO: ultrafast transient absorption.**

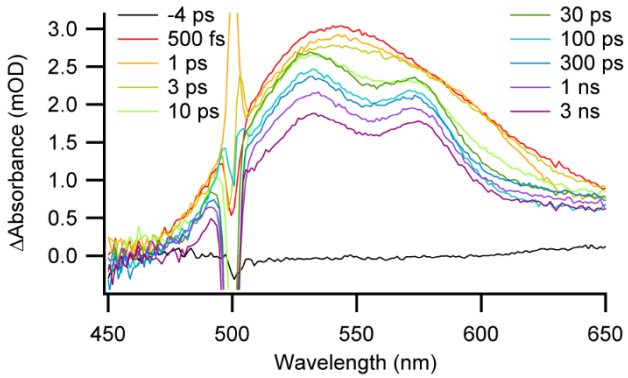


**Figure S29.** Ultrafast transient absorption spectrum for **3** on 20 nm AAO.

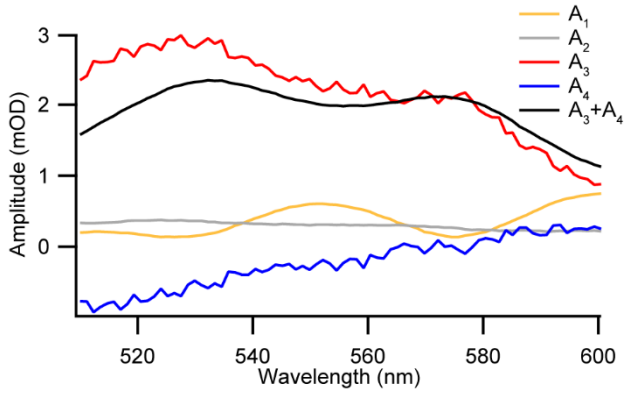


**Figure S30.** Global fit parameters from ultrafast transient absorption for **3** on 20 nm AAO (spectra in Figure 4).
$\tau_1$ = 8 ps
$\tau_2$ = 140 ps
$\tau_3$ = 18 ns (fixed based on nanosecond data)
$\tau_4$ = 120 ns (fixed based on nanosecond data)
fwhm = 300-400 fs
$A_1$, $A_2$, $A_3$, $A_4$ = shown as a function of wavelength
The lifetimes for the two longer time components were fixed based on nanosecond data. Because their lifetimes are far in excess of the experiment limits, their spectral components show some dependency (observed as equal and opposite apparent noise). Their sum is also shown, which reflects the spectral components observed on a nanosecond transient absorption spectrometer as in Figure S33.

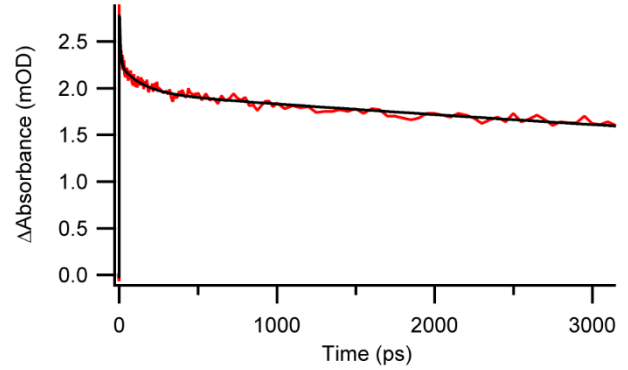


**Figure S31.** Kinetic trace at 555 nm for **3** on 20 nm AAO.

**Complex 3 immobilized on 20 nm AAO: nanosecond transient absorption.**

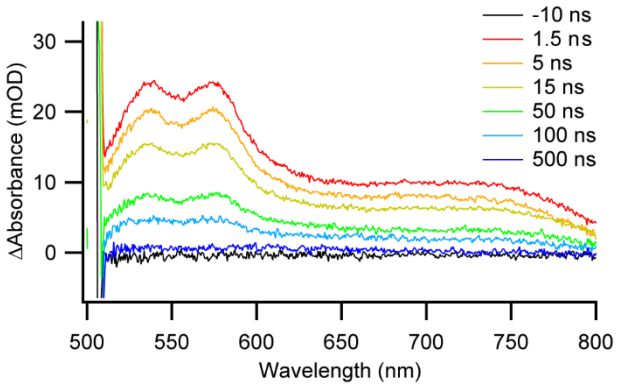


**Figure S32.** Nanosecond transient absorption spectrum for **3** on 20 nm AAO.

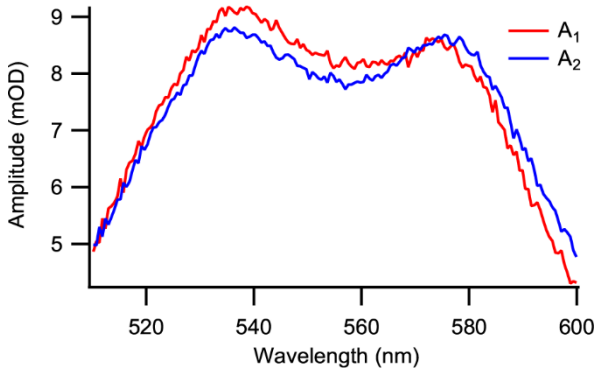


**Figure S33.** Global Fit Parameters from nanosecond transient absorption of **3** on 20 nm AAO.
$\tau_1$ = 18 ns
$\tau_2$ = 120 ns
fwhm = 1.0 ns
$A_1$, $A_2$ = shown as a function of wavelength

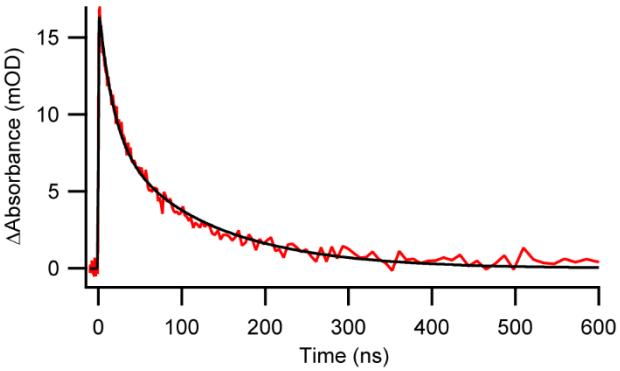


**Figure S34.** Kinetic trace at 575 nm for **3** on 20 nm AAO.

**Complex 3 immobilized on 10 nm AAO: ultrafast transient absorption.**

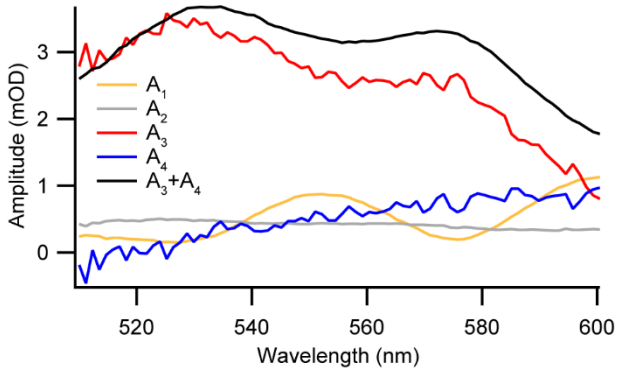


**Figure S35.** Global fit parameters for ultrafast transient spectra of **3** on 10 nm AAO.
$\tau_1$ = 8 ps
$\tau_2$ = 240 ps
$\tau_3$ = 16 ns (fixed based on nanosecond data)
$\tau_4$ = 120 ns (fixed based on nanosecond data)
fwhm = 300-400 fs
$A_1$, $A_2$, $A_3$, $A_4$ = shown as a function of wavelength
The lifetimes for the two longer time components were fixed based on nanosecond data. Because their lifetimes are far in excess of the experiment limits, their spectral components show some dependency (observed as equal and opposite apparent noise). Their sum is also shown, which reflects the spectral components observed on a nanosecond transient absorption spectrometer as in Figure S38.

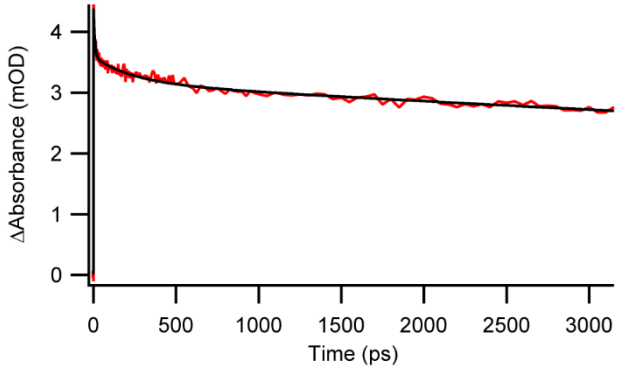


**Figure S36.** Kinetic trace at 555 nm for **3** on 10 nm AAO.

**Complex 3 immobilized on 10 nm AAO: nanosecond transient absorption.**

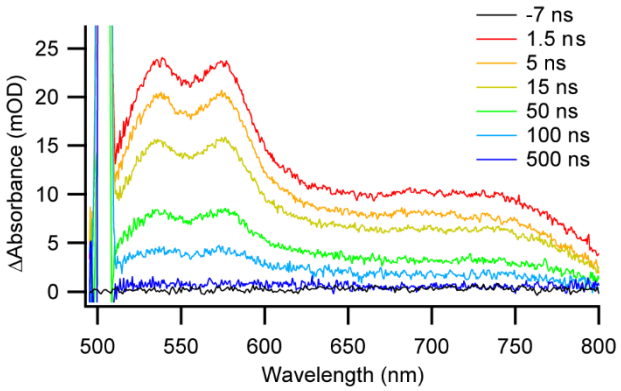


**Figure S37.** Nanosecond transient absorption spectrum for **3** on 10 nm AAO.

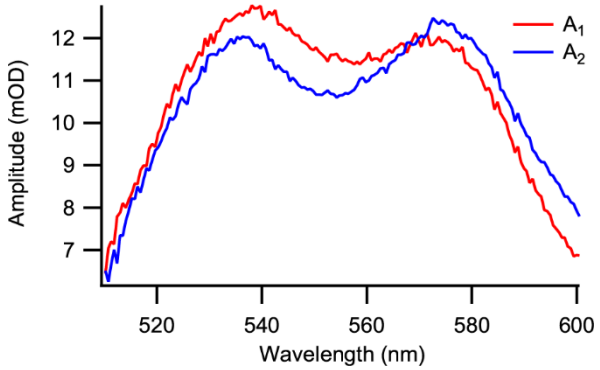


**Figure S38.** Global fit parameters for nanosecond transient absorption of **3** on 10 nm AAO.
$\tau_1$ = 16 ns
$\tau_2$ = 120 ns
fwhm = 1.0 ns
$A_1$, $A_2$ = shown as a function of wavelength

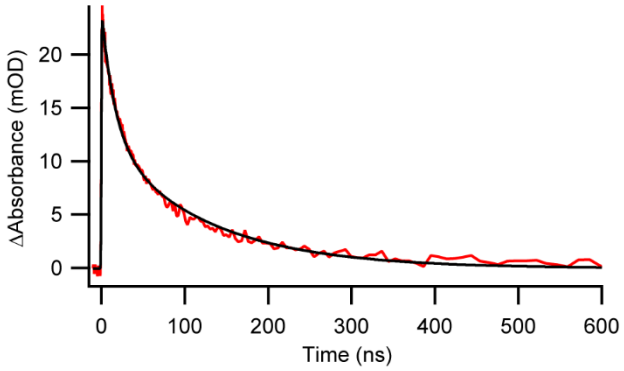


**Figure S39.** Kinetic trace at 575 nm for **3** on 10 nm AAO.

**Complex 3 immobilized on nanoparticle $TiO_2$ film: nanosecond transient absorption.**

For **3** immobilized on $TiO_2$ nanoparticle films, single wavelength data were fit to equation S4. we observed a small excited-state population which decays with an average lifetime of 5 ns. This is likely due to a population of non-injecting **3** rather than reflective of the injection kinetics which are likely to occur on a timescale faster than the instrument response.

$$y = y_0 + \sum_n A_n \exp\left\{\frac{-(t-t_0)}{\tau_n}\right\} \quad \text{(S4)}$$

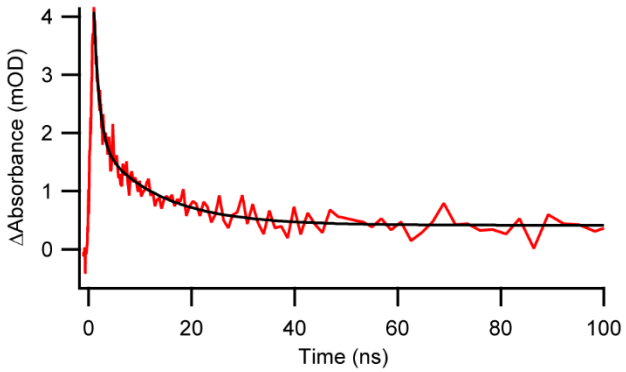


**Figure S40.** Decay of transient absorbance signal at 575 nm for **3** immobilized on $TiO_2$ films immersed in $CH_2Cl_2$.
$t_0$ = 1 ns
$y_0$ = 0.41 (mOD)
$\tau_1$ = 1 ns
$\tau_2$ = 12 ns
$\tau_{avg}$ = 5 ns
$A_1$ = 2.22 (mOD)
$A_1$ = 1.45 (mOD)

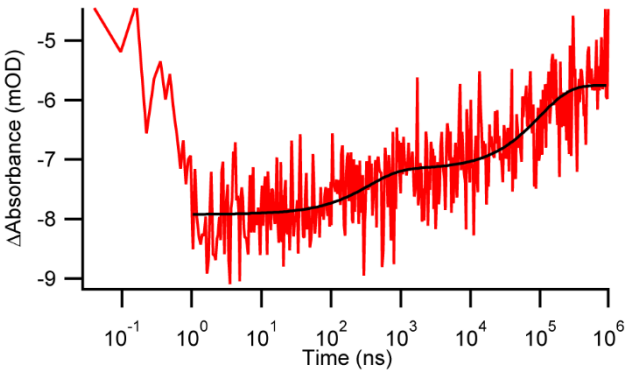


**Figure S41.** Recovery of MLCT bleach at 480 nm for **3** immobilized on $TiO_2$ films immersed in $CH_2Cl_2$.
$t_0$ = 1 ns
$y_0$ = -5.75 (mOD)
$\tau_1$ = 450 ns
$\tau_2$ = 115 µs
$\tau_{avg}$ = 75 µs
$A_1$ = 0.77 (mOD)
$A_1$ = 1.42 (mOD)

**References**


1. N. G. Connelly and W. E. Geiger, *Chem. Rev.*, 1996, **96**, 877-910.
2. S. R. Greenfield and M. R. Wasielewski, *Opt. Lett.*, 1995, **20**, 1394-1396.
3. D. Hayes, L. Kohler, R. G. Hadt, X. Zhang, C. Liu, Karen L. Mulfort and L. X. Chen, *Chem. Sci.*, 2018, **9**, 860-875.
4. L. Wang, N. P. Brawand, M. Vörös, P. D. Dahlberg, J. P. Otto, N. E. Williams, D. M. Tiede, G. Galli and G. S. Engel, *Adv. Opt. Mater.*, 2018, **6**, 1700975.
5. L. Kohler, D. Hayes, J. Hong, T. J. Carter, M. L. Shelby, K. A. Fransted, L. X. Chen and K. L. Mulfort, *Dalton Trans.*, 2016, **45**, 9871-9883.
6. M. Yanagida, L. P. Singh, K. Sayama, K. Hara, R. Katoh, A. Islam, H. Sugihara, H. Arakawa, M. K. Nazeeruddin and M. Grätzel, *J. Chem. Soc., Dalton Trans.*, 2000, DOI: 10.1039/B002391O, 2817-2822.
7. Y. Shigeta, A. Kobayashi, T. Ohba, M. Yoshida, T. Matsumoto, H.-C. Chang and M. Kato, *Chem. Eur. J*, 2016, **22**, 2682--2690.
8. H. Wolpher, S. Sinha, J. Pan, A. Johansson, M. J. Lundqvist, P. Persson, R. Lomoth, J. Bergquist, L. Sun, V. Sundström, B. Åkermark and T. Polívka, *Inorg. Chem.*, 2007, **46**, 638-651.
9. D. G. McCafferty, B. M. Bishop, C. G. Wall, S. G. Hughes, S. L. Mecklenberg, T. J. Meyer and B. W. Erickson, *Tetrahedron*, 1995, **51**, 1093-1106.
10. K. Hara, H. Sugihara, L. P. Singh, A. Islam, R. Katoh, M. Yanagida, K. Sayama, S. Murata and H. Arakawa, *J. Photochem. Photobiol. A*, 2001, **145**, 117-122.
11. R. H. Zheng, H. C. Guo, H. J. Jiang, K. H. Xu, B. B. Liu, W. L. Sun and Z. Q. Shen, *Chin. Chem. Lett.*, 2010, **21**, 1270-1272.
12. B. H. Farnum, K.-R. Wee and T. J. Meyer, *Nat. Chem.*, 2016, **8**, 845--852.
13. B. O'Regan, J. Moser, M. Anderson and M. Graetzel, *J. Phys. Chem.*, 1990, **94**, 8720-8726.
14. T. A. Heimer, S. T. D'Arcangelis, F. Farzad, J. M. Stipkala and G. J. Meyer, *Inorg. Chem.*, 1996, **35**, 5319-5324.
15. B. J. Hathaway and D. E. Billing, *Coord. Chem. Rev.*, 1970, **5**, 143-207.
16. J. R. Pilbrow, *Transition Ion Electron Paramagnetic Resonance*, Oxford University Press, 1991.